ETH
Eidgenössische Technische Hochschule Zürich
Swiss Federal Institute of Technology Zurich

IAC Institute for Atmospheric and Climate Science

Master's Thesis

The role of cold and warm air advection for the hydrological cycle in the South Indian Ocean

Department of Earth Sciences, ETH Zurich
Institute for Atmospheric and Climate Science

Iris Thurnherr, Institute for Atmospheric and Climate Science, ETH Zurich (main advisor)
Dr. Franziska Aemisegger, Institute for Atmospheric and Climate Science, ETH Zurich
Natalia Machado Crespo, Institute for Atmospheric and Climate Science, ETH Zurich and Institute for Astronomy, Geophysics and Atmospheric Sciences, University São Paulo

Submitted by

Katharina Hartmuth
14-942-437
Zurich, March 29, 2019

Abstract

This Master's Thesis investigates the role of cold air advection (CAA) and warm air advection (WAA) for freshwater fluxes in the South Indian Ocean. A feature-based method is developed and applied to ERA-Interim reanalysis data of the European Centre for Medium Range Weather Forecasts. Regions of CAA and WAA are diagnosed using an objective identification scheme based on a threshold of the near-surface temperature gradient between the ocean and the atmosphere. This identification method is first tested for a case study of an extratropical cyclone passage in the South Indian Ocean in January 2017. Then a climatology of CAA and WAA is established and typical environmental conditions associated with CAA and WAA are identified. The structure of the storm track is strongly imprinted on CAA and WAA frequency in the mid-latitudes. Strong WAA occurs mainly in the warm sector of cyclones, whereas CAA occurs in the cold sector of cyclones as well as over large parts of the subtropical anticyclone belt. The climatological frequency of CAA events is further affected by the warm Agulhas current to the southeast of South Africa and the Antarctic sea-ice extent in the framework presented here for identifying these events. A strong asymmetry towards higher CAA frequencies than WAA frequencies can be observed which is particularly pronounced during winter due to the large heat capacity of the ocean compared to the fast radiative cooling of the atmosphere. This difference in heat capacity is responsible for the fact that the atmosphere is generally colder than the ocean even without advection. Using backward trajectories and a composite analysis of conditions during CAA and WAA, areas of CAA are found to be characterized by strong evaporation fluxes leading to extensive atmospheric moisture uptake whereas WAA enhances dew formation and precipitation. The analysis of the stable water isotope (SWI) composition in monthly precipitation from data of the Global Network of Isotopes in Precipitation on Marion Island in combination with a moisture source diagnostic reveals the dominance of CAA in the moisture source region, which is located in the area of the Agulhas current. A positive correlation between CAA frequency at the moisture source and the d-excess in precipitation can be observed. CAA variability, resulting from seasonal changes in CAA frequency and the spread of the moisture uptake location, determines the variability of the humidity gradient at the moisture source and thus affects the non-equilibrium fractionation conditions in the moisture source area. The detailed analysis of air-sea interactions during CAA and WAA events combined with the evaluation of SWI data underlines the importance of CAA and WAA for the hydrological cycle in the South Indian Ocean.

Abbreviations

d Deuterium Excess

q Specific Humidity

CAA Cold Air Advection

CP Convective Precipitation

E Evaporation

ECMWF European Centre for Medium range Weather Forecast

D Dew deposition

GNIP Global Network of Isotopes in Precipitation

LSP Large-Scale Precipitation

LWC Liquid Water Content

MAI Monthly Advection Index

MI Marion Island

P Precipitation

PBL Planetary Boundary Layer

RH Relative Humidity

SAWS South African Weather Service

SLHF Surface Latent Heat Flux

SLP Sea Level Pressure

SSHF Surface Sensible Heat Flux

SST Sea Surface Temperature

SWI Stable Water Isotopes

UTC Coordinated Universal Time

WAA Warm Air Advection

ZAA Zonal Air Advection

Contents

1 Introduction

1.1 Background

Meridional heat transport by synoptic atmospheric systems is an important driving mechanism for strong transient fluxes of heat and moisture between the ocean and the atmosphere. Advection of warm air over a relatively colder ocean surface or cold air over a relatively warmer ocean surface by cyclones or their frontal systems leads to heat and generally also moisture fluxes due to the thermodynamical disequilibrium between the two phases (Fig. 1). Freshwater fluxes in the form of evaporation (E), precipitation (P) and dew deposition (D) ensue, thus coupling the energy and water budgets of the atmosphere and the ocean. E leads to energy and water loss of the ocean and thus energy and water input into the atmosphere whereas D leads to energy and water loss of the atmosphere and water input into the ocean. P leads to water loss of the atmosphere and water input into the ocean. Large-scale E plays a fundamental role for ocean deep convection events and transfer of latent heat into the atmosphere, whereas freshwater input in the form of P is important for the formation rates of oceanic water masses (Talley, 2008). The net surface freshwater flux into the atmosphere is defined as E-P and is one of the key parameters in the hydrological cycle.

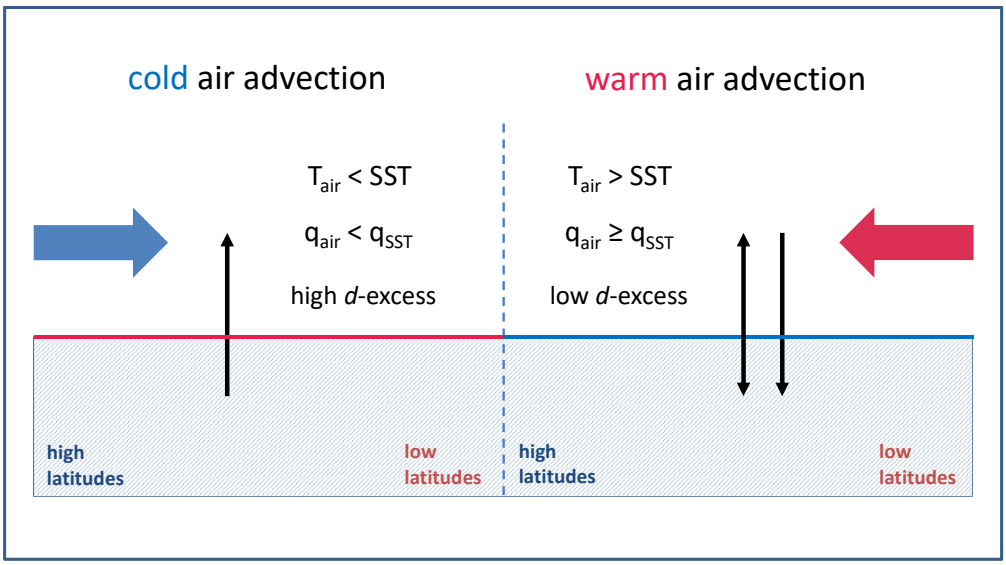

Figure 1: Conditions during cold air advection (CAA, left) and warm air advection (WAA, right). Arrows indicate the direction of E (during CAA) and E, D and P (during WAA), respectively. Conditions are represented by temperature and specific humidity of the air mass (T_{air} and q_{air}) and at the sea surface (SST and q_{SST}).

Several studies have focused on the role of weather systems like cyclones or fronts for freshwater fluxes, especially in the Southern Hemisphere (Papritz et al., 2014, 2015).

Advection of cold and warm air masses, which is often linked to cyclones and their fronts, is thus expected to play a key role for the temporal and spatial variability of freshwater fluxes. Figure 1 shows theoretically expected features of cold air advection (CAA) and warm air advection (WAA) regarding air-sea interaction. In case of CAA, the air temperature is lower than the sea surface temperature (SST) and the air is undersaturated with respect to the sea surface. As a consequence, strong non-equilibrium conditions, resulting in latent and sensible heat fluxes from the ocean to the atmosphere are expected. On the contrary, if warm air is transported over a relatively cooler ocean surface, the air is close to or above saturation. Freshwater fluxes into the atmosphere are assumed to be suppressed as dew formation and precipitation are advantaged in such conditions.

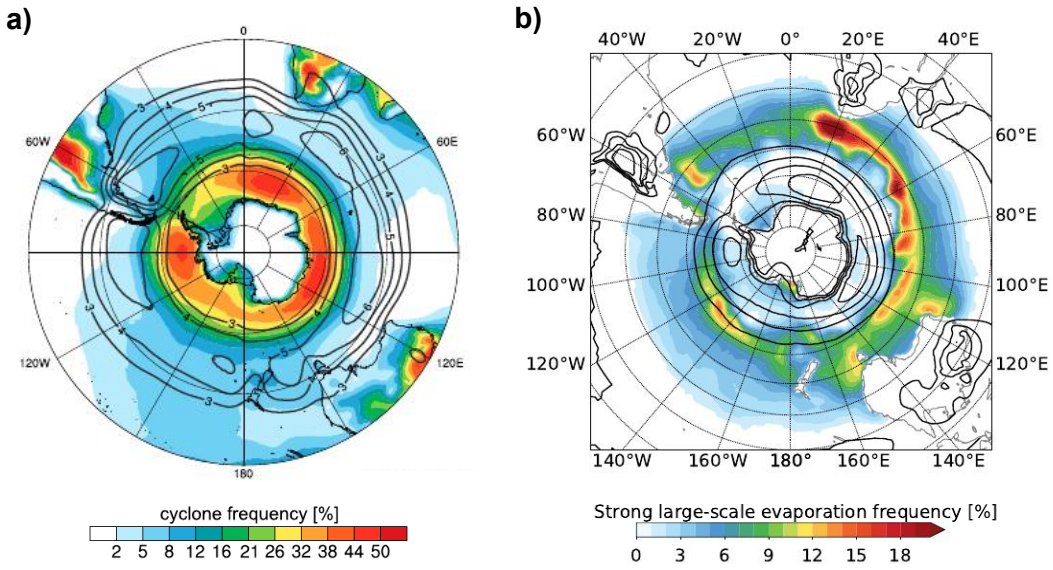

Figure 2: (a) Climatological cyclone frequency (%; shaded) and front frequency (%; dark gray contour lines) during austral summer (DJF) averaged over the period 1980-2010 (from Papritz et al., 2014). (b) Climatological strong ocean evaporation frequency (%; shaded) and cyclone frequency (black contour lines) for DJF averaged over the period 1979-2014 (from Aemisegger and Papritz, 2018).

Several studies reveal that advection of cold, dry air from the Antarctic continent triggers evaporation events, especially in winter (Bracegirdle and Kolstad, 2010; Papritz et al., 2015). Strong large-scale ocean evaporation events are thus frequently associated with the passage of extratropical cyclones (Fig. 2b) due to the advection of cold and dry air at the rearward side of the cyclone (Aemisegger and Papritz, 2018). On the contrary, the frequent advection of warm, humid air from the subtropics and the southern parts of the mid-latitudes in the warm sector of cyclones inhibits the formation of such events (Aemisegger and Papritz, 2018) and leads to ascending air masses on the large-scale and precipitation (Madonna et al., 2014; Pfahl et al., 2014). Therefore, the cold and

warm sectors of extratropical cyclones are expected to show distinct and contrasting features in terms of air-sea fluxes and near-surface thermodynamic conditions.

In the southern part of the Indian Ocean and the eastern South Atlantic, a year-round maximum of cyclone and front frequency is located (Fig. 2a). At the same time, the highest frequency of strong large-scale evaporation events in the Southern Ocean could be detected, induced by CAA (Aemisegger and Papritz, 2018; Fig. 2b). Next to the CAA and WAA directly related to the passage of extra-tropical cyclones, the South Indian Ocean features CAA due to exceptionally cold air masses over Antarctica and ocean currents. The warm Agulhas current to the east of South Africa has shown significant effects on the local freshwater fluxes (Rouault et al., 2002). Along the Antarctic coast line, CAA events are related to cold air outbreaks which advect very cold and dry air masses over the Southern Ocean resulting in strong latent and sensible heat fluxes from the ocean into the atmosphere (Papritz et al., 2014). The interplay between the storm track, the ocean currents and the subtropical anticyclones as well as the influence of the Antarctic and African continental landmasses make this region very attractive for further examination.

In the region of the South Indian Ocean, large-scale E and P events can have an important impact on the hydrological cycle. The production of sinking water masses in the Southern Ocean depends mainly on the ocean stratification, which has been shown by Lovenduski and Ito (2009) to be highly sensitive to changes in E-P. 60% to 90% of the total freshwater flux in this region can be attributed to extratropical cyclones and fronts (Papritz et al., 2014). The same study could also show that in the South Indian Ocean fronts are more important for strong precipitation events than in the remaining Southern Ocean, where cyclones are dominating the contribution to strong precipitation events. Thus, it will be interesting to investigate the role of CAA and WAA in this thesis not only for air-sea interaction in cyclones, but also as drivers of regional precipitation patterns.

The accumulation of exceptional features such as the Southern Hemispheric storm track and the Agulhas current in the South Indian Ocean combined with its relevance for oceanic surface stratification and extreme E and P events makes it crucial to better understand the complex interplay of the driving factors of air-sea interactions in this region. A systematic and feature-based investigation of the influence of CAA and WAA on air-sea fluxes over a mainly oceanic region like the Southern Ocean has not been carried out so far. A detailed case study analysis combined with a climatology of CAA and WAA frequency and associated air-sea interactions will improve our understanding of the processes affecting the hydrological cycle in one of the most important oceanic regions.

To gain more insight into moisture source regions and transport processes, the isotopic composition of precipitation will be analyzed. Stable water isotopes (SWI) are natural

tracers of moist atmospheric processes. The thermodynamic disequilibrium between ocean and atmosphere during CAA and WAA should thus be reflected in distinct, measurable isotope signals in the atmosphere. The most important stable water isotopologues are $H_2{}^{18}O$ and $HD^{16}O$. The SWIs are commonly expressed with the δ-notation, which is defined as the isotopic ratios normalized to a reference isotopic standard ratio:

$$\delta^{18}\mathrm{O} = \left(\frac{\left(\frac{\mathrm{H_2{}^{18}O}}{\mathrm{H_2{}^{16}O}}\right)_{\mathrm{sample}}}{\left(\frac{\mathrm{H_2{}^{18}O}}{\mathrm{H_2{}^{16}O}}\right)_{\mathrm{ref}}} - 1\right) \cdot 1000‰ \tag{1}$$

$$\delta\mathrm{D} = \left(\frac{\left(\frac{\mathrm{HD^{16}O}}{\mathrm{H_2{}^{16}O}}\right)_{\mathrm{sample}}}{\left(\frac{\mathrm{HD^{16}O}}{\mathrm{H_2{}^{16}O}}\right)_{\mathrm{ref}}} - 1\right) \cdot 1000‰ \tag{2}$$

As a reference ratio, the Vienna Standard Mean Ocean Water (VSMOW2) is used.

Distinct isotope signatures associated with cyclones and fronts have been previously described using measurements as well as model simulations. High values of δ^{18}O can be observed in the warm sector of cyclones with a progressive depletion during the cold front passage, leading to low δ^{18}O values in the cold sector (Gedzelman and Lawrence, 1990; Pfahl et al., 2012; Aemisegger et al., 2015; Dütsch et al., 2016). Areas of WAA are thus expected to show high values of δ^{18}O compared to lower δ^{18}O values in regions where CAA dominates. Furthermore, Gedzelman and Lawrence (1990) associated enriched δ^{18}O values with convective precipitation, which experienced little prior fractionation, in the warm sector. Stratiform precipitation behind the cold front showed significantly lower δ^{18}O values. CAA and WAA events have also been identified in marine boundary layer water vapour from ship-based SWI measurements during the Antarctic Circumnavigation Expedition (ACE) in the Southern Ocean (PhD Iris Thurnherr, personal communication, [1]).

A further measure, which is an important tracer for non-equilibrium processes and thus particularly useful as proxy for ocean evaporation or dew deposition is the deuterium excess (d). It is defined as

$$d = \delta\mathrm{D} - 8 \cdot \delta^{18}\mathrm{O} \tag{3}$$

and describes the relative enrichment of the $HD^{16}O$ molecules compared to 8 times the number of the $H_2{}^{18}O$ molecules in a given vapour or precipitation sample. d is 0 ‰ for ocean water or vapour in equilibrium over the ocean surface. Non-equilibrium isotope fractionation is mainly determined by the ocean-atmosphere humidity gradient and the SST (Merlivat and Jouzel, 1979; Uemura et al., 2008). d is thus an important indicator for fluxes in areas of CAA, where the specific humidity gradient at the ocean surface is large (Aemisegger and Sjolte, 2018). Moisture diffusion and thus high d values are expected in the evaporate. On the contrary areas of WAA, where often saturation or

even supersaturation relative to the SST occurs, are expected to show a low or even negative d in vapour (Fig. 1).

It is still not fully understood which processes dominate the SWI variability of atmospheric moisture on different time scales. Furthermore, the influence of CAA and WAA events on moisture uptake and their representation in precipitation measurements is not well understood yet. In this Master's Thesis, precipitation isotope samples from Marion Island (MI) will be used to investigate how the integrated effect of CAA and WAA events is reflected in the SWI of monthly precipitation. The hypothesis will be tested whether monthly precipitation isotopes could potentially represent a measureable validation proxy for the occurrence frequency of CAA and WAA in the South Indian Ocean. Combined with the case study analysis and the climatology, the evaluation of SWI measurements will provide new insights regarding the processes affecting air-sea interactions and SWI variability in the South Indian Ocean.

1.2 Objectives and Goals

In this Master's Thesis the influence of advection of cold and warm air masses over relatively warmer and colder ocean surfaces, respectively on E, P and D over the South Indian Ocean is investigated. ERA-Interim reanalysis data (Dee et al., 2011) will be used to carry out a case study and generate a climatology of CAA and WAA in the South Indian Ocean. The aim is to deal with the following research questions:

1. Which type of air-sea interactions are typically observed during CAA and WAA?
2. What is the spatial and temporal distribution of CAA and WAA events in different seasons?
3. Is the frequency of CAA and WAA represented in the SWI composition of monthly precipitation?

A climatology of CAA and WAA for the Southern Ocean will bring new insights into the connection of air-sea interaction and the large-scale forcing by the advection of cold and warm air masses in extratropical cyclones. Furthermore, combining reanalysis data with stable water isotope measurements will provide a better understanding of the isotopic signature of synoptical systems and their impact on the monthly isotopic composition of precipitation.

2 Data Sets and Methods

2.1 Data Sets

Two distinct and independent data sets will be used in this Master's Thesis. For the case study analysis and the climatology calculation the ERA-Interim reanalysis data set (Dee et al., 2011) of the European Centre for Medium range Weather Forecast (ECMWF) will be used. The data is available for the period 1979 to 2017 with a 6h temporal resolution. The atmospheric fields are interpolated to a 1°x1° horizontal grid with 60 vertical levels. Due to limited spatiotemporal resolution and lack of observations, especially on the Southern Hemisphere, uncertainties in the reanalysis data have to be considered. The correct approximation of surface fluxes over the ocean is dependent on the SST data which often is not sufficiently high resolved to represent meso-scale air-sea interaction as exact as possible (Rouault et al., 2003). However, using a continuous data set with instantaneous fields for multiple variables allows the fairly accurate calculation of a climatology of large-scale CAA and WAA in this thesis.

The link of CAA and WAA with the isotope signature of atmospheric waters will be evaluated using monthly isotope data from the Global Network of Isotopes in Precipitation (GNIP, [2]) (Araguás-Araguás et al., 2000) station Marion Island (46°88'S and 37°87'E) in the South Indian Ocean. The GNIP isotope and precipitation data is available for the periods 1993-2001 and 2009-2012. In addition, daily precipitation measurements from the South African Weather Service (SAWS, [3]) on MI is used to examine the reliability of the GNIP data set. Therefore, a comparison of the monthly GNIP and SAWS precipitation data is performed.

Figure 3a shows that both data sets coincide rather well. Data points for which GNIP and SAWS precipitation rates differ by more than 20% are discarded. For a model evaluation, the monthly precipitation of the ERA-Interim reanalysis data and the GNIP data set are compared. As can be seen in Fig. 3b, the ERA-Interim data often underestimate the measured precipitation. This can be explained due to the topography of MI, which is not resolved in the ERA-Interim reanalysis data. Precipitation due to orographic enhancement on the island is thus underestimated in the reanalysis data.

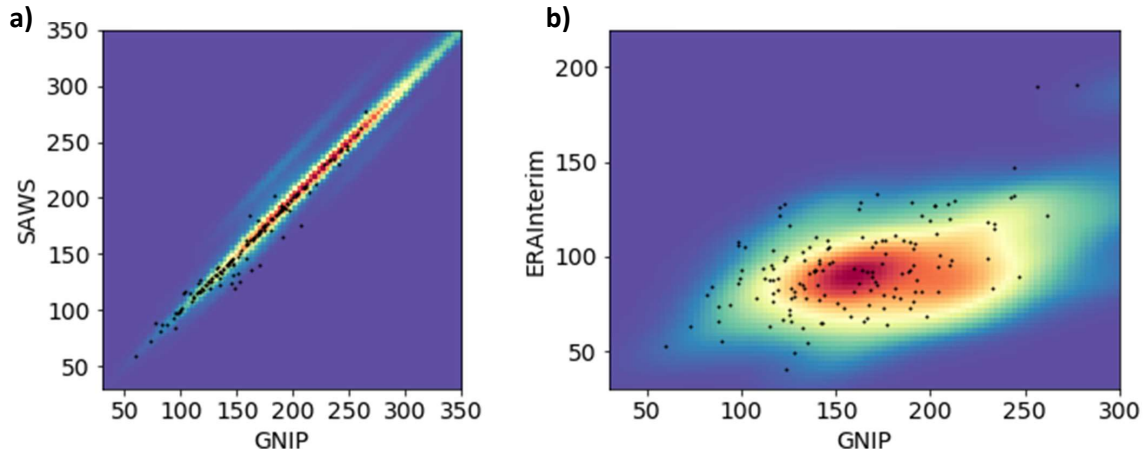

Figure 3: Density plot overlaid by scatter plot of monthly precipitation (mm) comparing (a) GNIP data with SAWS data, (b) GNIP data with ERA-Interim reanalysis data on MI.

2.2 Methods

2.2.1 Air Temperature Advection Identification Scheme

In the first part of this thesis, air-sea interactions associated with CAA and WAA are analyzed in a case study from the Antarctic Circumnavigation Expedition (ACE, [1]) in January 2017. The event occurred in the region of the South Indian Ocean (section 3). To define areas of CAA and WAA, an objective identification scheme is applied based on ERA-Interim reanalysis data. The type of advection is given by the temperature gradient between the atmosphere and the ocean, which is in this case defined as the difference between the 10 m temperature ($T_{10\mathrm{m}}$) and the SST, $\Delta T = T_{10\mathrm{m}}$-SST. Areas, in which $T_{10\mathrm{m}}$-SST>0, describe in general areas of WAA, where the air temperature is larger than the SST and the air is close to or above saturation (Fig. 1, right panel). As a consequence, latent and sensible heat fluxes into the atmosphere are small or even directed into the ocean and such events are often accompanied by P. The freshwater flux associated with WAA is thus expected to generally consist of two parts: precipitation and vapour deposition. In areas where $T_{10\mathrm{m}}$-SST<0, the air temperature is lower than the SST and thus near-surface CAA occurs (Fig. 1, left panel). In this case, the air is undersaturated with respect to the sea surface and, consequently, latent and sensible heat fluxes from the ocean to the atmosphere occur.

To distinguish between cases of weak temperature advection with approximately zonal flow from events with clear temperature advection, the thresholds of ±1K are applied. If the temperature difference is smaller than 1K, the term zonal air advection (ZAA) is used. It has to be noted that CAA and WAA is defined here from an air-sea interaction perspective, which is the reason why the vertical temperature gradient is used as an identification field.

To refine this scheme, an additional subdivision into areas of weak and strong temperature advection is made. Areas of strong WAA are defined for a temperature gradient T_{10m}-SST>2, whereas areas of weak WAA are defined for 2>T_{10m}-SST>1. Similarly, areas of strong CAA are defined with T_{10m}-SST<-2 and areas of weak CAA with -2<T_{10m}-SST<-1. A visualization of this scheme is shown in Fig. 4. As this thesis deals exclusively with the oceanic part of the hydrological cycle, areas of land as well as areas where the amount of sea-ice is above 50% are excluded from the identification scheme.

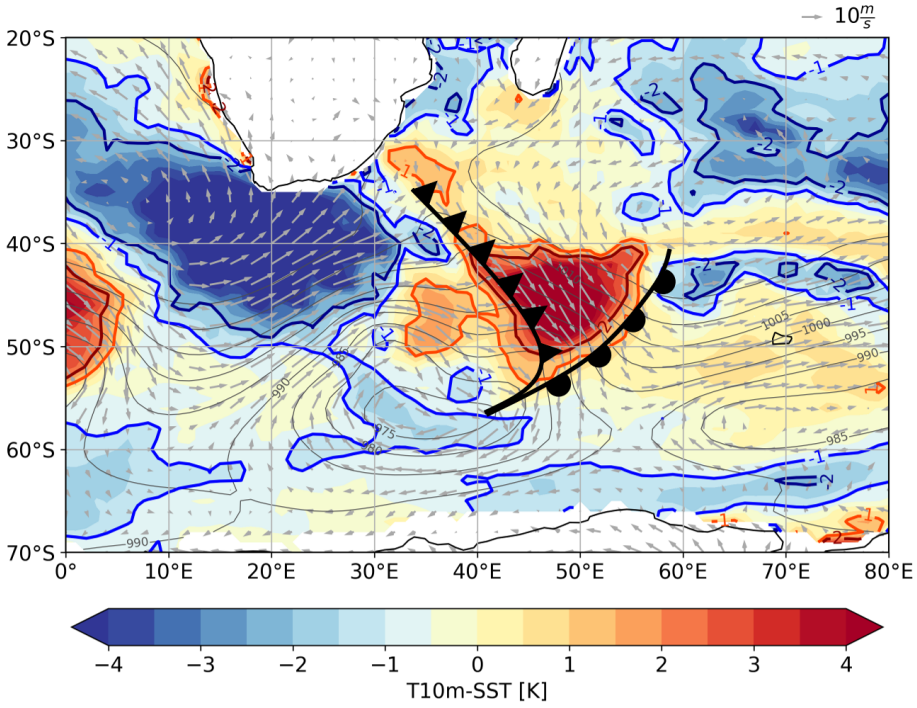

Figure 4: Objective Identification of Temperature Advection. Difference between T_{10m} and SST (K; shaded), sea level pressure SLP (hPa; black contour lines with a 5 hPa interval) and horizontal wind at 10m (m/s; grey arrows) from ECMWF operational data at 06 UTC 03 Jan 2017. Areas of strong and weak WAA and strong and weak CAA, respectively, are shown (dark red, red, dark blue and blue contour lines). The position of the primary warm front and primary cold front of the cyclone is indicated (black weather map symbol).

2.2.2 Mean Conditions during CAA and WAA

The advection identification scheme is applied to ERA-Interim reanalysis data for the period 1979-2016 to generate a climatology of CAA and WAA in the South Indian Ocean for the study area between 20°S and 70°S and 0° and 80°E. The frequency of CAA and WAA events is analyzed as well as the air-sea fluxes associated with the events. To do this, conditional average fields of the latent heat flux (SLHF) which can be converted to E and D and the sensible heat flux (SSHF) as well as convective precipitation (CP)

and large-scale precipitation (LSP) are compiled for CAA and WAA events. Further variables which are investigated are the SST and the relative humidity with respect to the SST (RH_{SST}). The advection identification scheme (section 2.2.1) is used to define for each grid point and time if there is an area of CAA, WAA or ZAA. It has to be mentioned that the number of available data per advection type differs between the grid points, as the frequency of CAA, WAA and ZAA varies widely (section 4.2). This needs to be considered when analyzing the climatological mean values (section 4.3). As for the advection identification scheme, fluxes over land as well as in regions with a sea-ice ratio of over 50% are neglected. These areas are flagged as white areas for all variables. For the seasonal mean conditions, the sea-ice extent varies and thus also the flagged area.

2.2.3 Monthly Advection Index

In the last part of the thesis, SWI data from monthly accumulated precipitation sampled on MI for the periods 1993-2001 and 2009-2012 is used to analyze the synoptic imprint of CAA and WAA on the isotope measurements. The SWI data includes measurements of the water vapour isotopologues $H_2{}^{18}O$ and $HD^{16}O$.

A monthly index for the relation of CAA and WAA is designed to analyze the influence of CAA and WAA on the isotopic composition of the monthly precipitation samples. A monthly advection index (MAI) is defined and calculated with the advection frequency on MI as follows:

$$\mathrm{MAI} = \ln\left(\frac{\mathrm{f_{WAA}}}{\mathrm{f_{CAA}}}\right) \tag{4}$$

$\mathrm{f_{WAA}}$ describes the monthly WAA frequency and $\mathrm{f_{CAA}}$ similarly the monthly CAA frequency. If MAI is positive/negative, MI experienced more WAA/CAA events during the specific month, respectively.

To calculate the MAI for MI, the ERA-Interim reanalysis data needs to be interpolated for the coordinates of the island. The data is interpolated only horizontally, as for the advection identification scheme only parameters of the lowest model level are required.

2.2.4 Trajectory Calculation

Backward trajectories are calculated to investigate the moisture origin during CAA and WAA events for the case study as well as for the station on MI. The 10-days backward trajectories are calculated with the Lagrangian analysis tool LAGRANTO 2.0 (Wernli and Davies, 1997; Sprenger and Wernli, 2015). For the case study, trajectories are separately calculated starting from areas of CAA and WAA in 6-hourly steps between 18 UTC 01 Jan 2017 and 06 UTC 04 Jan 2017. Additional 10-days forward trajectories are calculated to investigate not only the history of those air masses but also their future

development. Along the trajectories, parameters such as pressure, specific humidity (q), relative humidity (RH), liquid water content (LWC) and temperature are traced. To be able to compare the pressure in the air parcels relative to the pressure at the surface on their arrival point, p along the air parcel is normalized, using the following approach,

$$\mathrm{p_{norm}} = \mathrm{p_{air\ parcel}} \cdot \frac{1000\mathrm{hPa}}{\mathrm{p_0}} \tag{5}$$

where $\mathrm{p_0}$ denotes the surface pressure on MI at the arrival of the air parcel.

For the isotope analysis, trajectories are calculated from the location of the station of MI between a height of 1000 and 300hPa for 40 vertical layers for the duration of available isotope data (1993-2001 and 2009-2012). Only for air parcels which precipitate when reaching MI, backward trajectories are further evaluated, as only in these cases isotope data in precipitation is available. Multiple parameters are traced along the trajectories including $\mathrm{RH_{SST}}$ and the CAA, WAA and ZAA masks. To get a more detailed understanding of the link to the conditions at the moisture source, a Lagrangian moisture diagnostic as introduced in Sodemann et al. (2008) is performed. Based on the location of the air parcel in combination with its temperature, relative humidity and the change in its specific humidity, for every time step a process such as evaporation or cloud formation is allocated. As the moisture uptake occurs mainly by evaporation inside the planetary boundary layer (PBL), for this study, processes above the PBL such as mixing are neglected. If the specific humidity during one time step increases over a minimum uptake threshold ($\Delta q > \Delta q_{\mathrm{min}}$), the moisture increase is assigned to evaporation with Δq_{min}=0.1 g/kg, here. On the contrary, if ($\Delta q < -\Delta q_{\mathrm{min}}$), the air parcel looses moisture during that time step. Several events of moisture uptakes and moisture losses can occur during the 10-day transport. Thus, the signal of later moisture uptakes will be more dominant in the isotopic composition than the signal of earlier moisture uptakes which partially gets lost during moisture losses. To get the contribution of different moisture uptake events correctly, each moisture uptake is weighted with the fraction of moisture remaining in the air parcel at the arrival point. The later the moisture uptake happened and the larger Δq, the larger is its contribution to the final isotopic composition. The individual trajectories' contribution to the final six-hourly precipitation is defined by the specific humidity decrease in the last time step before arrival of the trajectory in MI. For obtaining monthly moisture source conditions and their geographical distribution, each six-hourly time step is weighted with the total surface precipitation interpolated to MI from the ERA-Interim data set. For more details on the procedure see Aemisegger (2018).

3 Case Study

In the first part of this thesis, a case study is performed to investigate the air-sea interactions associated with CAA and WAA induced by a cyclone. The event took place from 12 UTC on 01 Jan 2017 to 06 UTC on 06 Jan 2017 in an area between 30°S and 60°S and 0° and 70°E. During one week, an extratropical cyclone develops from a small low-pressure system (Fig. 5a) into a large and more stationary cyclone (Fig. 5f). The cyclone also develops a clear warm front as well as a primary and a weak secondary cold front. To better understand air-sea interactions in the context of CAA and WAA, several variables such as E and D, SSHF, RH_{SST} as well as CP and LSP are analyzed in the first part of the chapter. In the second part, backward trajectories are calculated to analyze the history and future of CAA and WAA air masses.

3.1 CAA and WAA in an Extratropical Cyclone

The objective advection identification scheme (section 2.2.1) has been used to identify regions of CAA and WAA in general and more specific regions of strong warm, weak warm, strong cold and weak cold air advection. Figure 5 shows the temperature gradient during the case study. An area of strong WAA can be identified in the region of the cyclone's warm sector southeast of the Cape of Good Hope. Behind the cold front, a larger area of strong CAA is visible which is wrapping around the Cape of Good Hope and extends far northwards into the subtropics. The areas of weak temperature advection are less distinct, but fit geographically well with the sectors of the cyclone. Further areas of weak CAA close to Antarctica can be associated with cold air outbreaks from the continent. In the subtropics, CAA is apparent as well, favoured by warm ocean currents west and east of South Africa (Fig. 7b) and the dominant anticyclone to the southeast of Madagaskar. During the case study, the areas of advection develop in size and strength similar to the size of the cyclone and reach their maximum extent between 00 UTC on 03 Jan and 12 UTC on 04 Jan 2017 (Figs. 5d, e). Especially, the shape of the WAA area coincides quite well with the warm sector of the cyclone. The area of CAA is however much larger and sometimes extends far outside the cyclone's cold sector. An interesting feature, which can also be seen in Fig. 4, is the common occurrence of weak WAA as well as CAA in the region between the first and the second cold front. This "false warm sector" between the primary cold front and a weaker secondary cold front is not clearly associated with either WAA or CAA exclusively but features both types of advection classes.

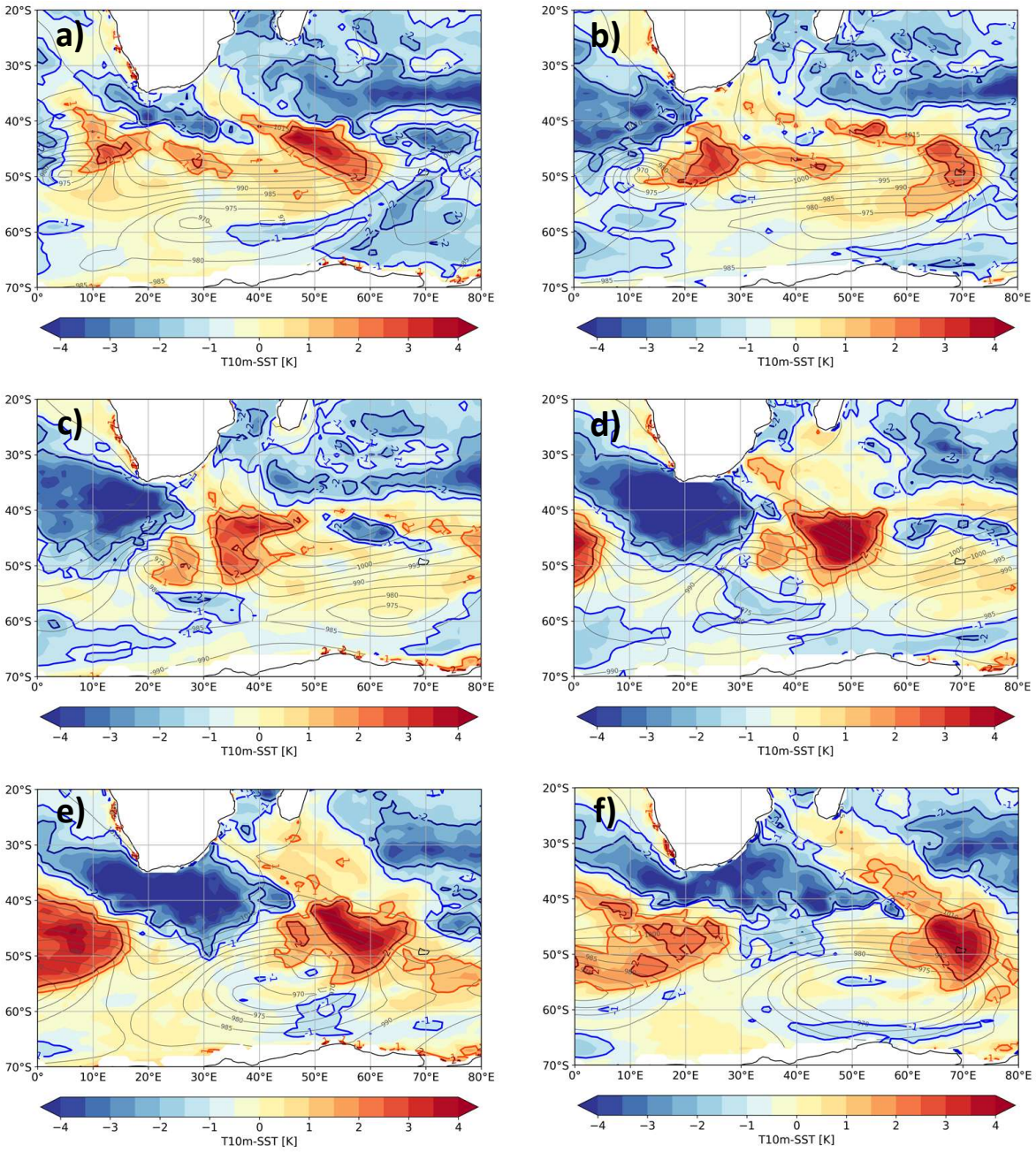

Figure 5: Temperature difference $T_{10\mathrm{m}}$-SST (K; shaded) and SLP (hPa; black contour lines with a 5 hPa interval) in 12-hourly steps between 18 UTC 01 Jan 2017 and 06 UTC 04 Jan 2017.

3.2 Air-Sea Interactions during CAA and WAA

Figure 6a shows the SSHF combined with the contour lines for CAA and WAA, respectively. As expected, there is a visible difference in direction and amount of the fluxes for the different air temperature advection areas. Areas of WAA correspond to positive sensible heat fluxes (directed into the ocean) whereas areas of CAA match negative sensible heat fluxes (directed into the atmosphere). For the duration of the case study, the maximum fluxes occur always in regions with strong CAA or WAA. In addition, the areas with the strongest fluxes coincide well with the cold and warm sector of the cyclone. It is evident that the cyclones are the main driver of the large-scale advection that induces the vertical temperature gradients and thus the heat exchange fluxes between the ocean and the atmosphere. Figure 6c shows that the maximum horizontal wind speed coincides with the regions of the strongest fluxes in SSHF (Fig. 6a) and E respectively D (Fig. 6b). Thus it seems clear that the temperature difference between ocean surface and atmosphere is mainly driven by advection in these areas.

The SLHF is used to calculate the evaporation and dew formation during the case study event, which is shown in Figure 6b. A general latitudinal gradient can be observed with higher values towards the tropics and lower values towards the Antarctic coast. This is due to the meridional temperature gradient and the temperature dependence of the saturation vapour pressure. Similar to the SSHF, the SLHF corresponds well with areas of CAA or WAA. In the warm sector mostly negative E indicates vapour deposition (D), whereas in the area of strong CAA, the highest values of E can be observed. However, it has to be mentioned that there is a strong asymmetry between E and D values as the usual humidity gradient at the sea surface favours E over D. As the cyclone is evolving and its cold and warm sector get more and more stretched (Fig. 5), the SLHF gets weaker and more patchy.

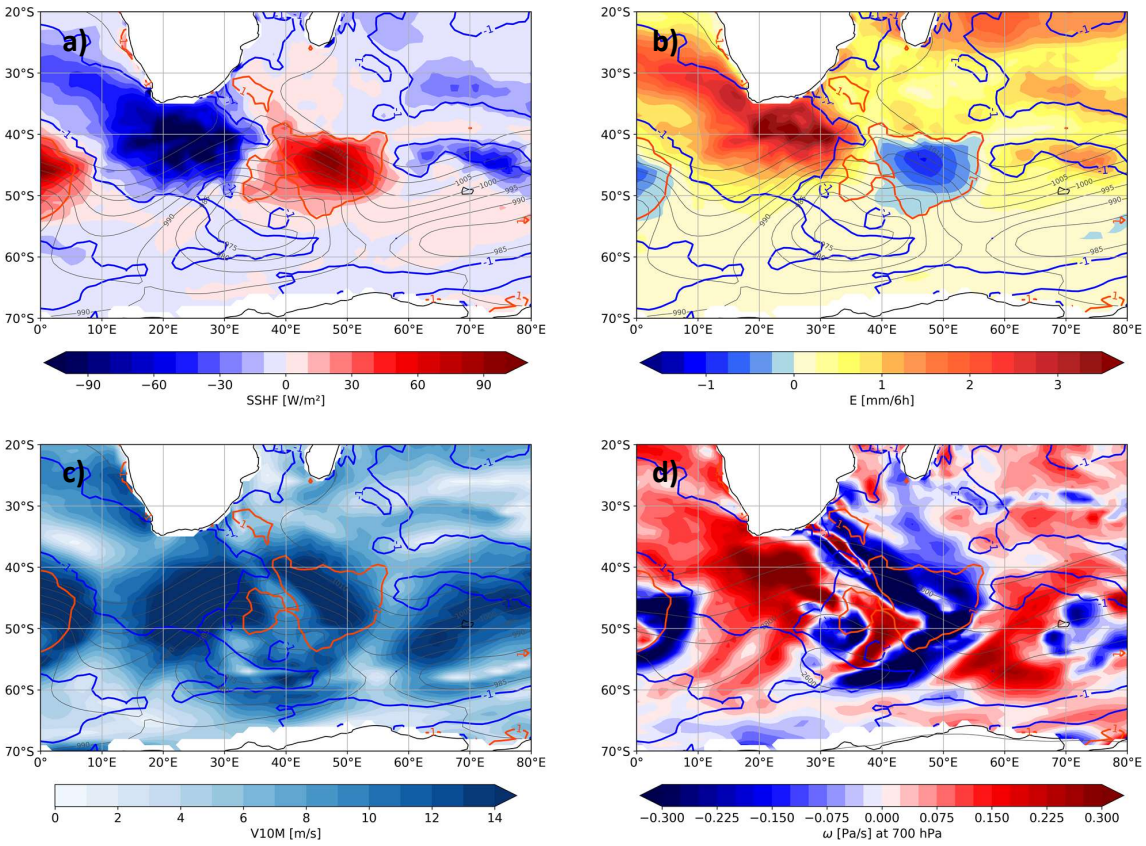

Figure 6: (a) SSHF (W/m^2; shaded), (b) E and D (mm/6h; shaded, positive values show E, negative values show D), (c) horizontal wind speed at 10m (m/s; shaded) with SLP (hPa; black contour lines with a 5 hPa interval) and (d) vertical wind speed ω at 700hPa (Pa/s; shaded) with geopotential (m; black contour lines with a 100 m interval) at 06 UTC 03 Jan 2017. Colored contour lines show areas of CAA (blue) and WAA (orange).

The RH_{SST} partly explains E and D, especially in regions of CAA or WAA. RH_{SST} is a measure for the saturation level of the atmosphere compared to a hypothetical thin saturated air layer at the ocean surface temperature. The warm sector of the cyclone shows for the most part RH_{SST} values above 100% (Fig. 7a), which indicates a supersaturation of the atmosphere compared to the sea surface (Fig. 7b) and explains the observed vapour deposition flux. By comparison, in the CAA area the RH_{SST} is relatively low with values between 40% and 60%, which is an important prerequisite for strong E. The primary cold front of the cyclone is associated with a strong gradient in RH_{SST}.

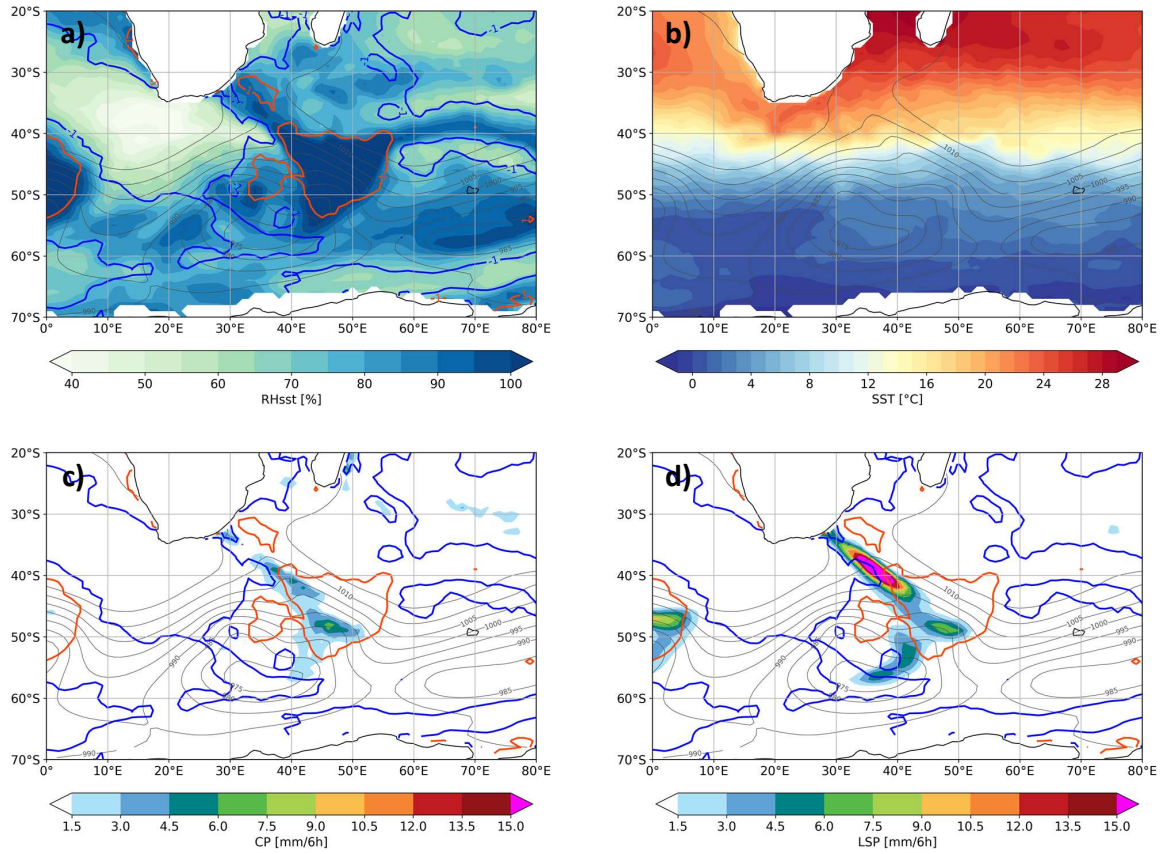

Figure 7: (a) RH_{SST} (%; shaded), (b) SST (°C; shaded), (c) CP (mm/6h; shaded) and (d) LSP (mm/6h; shaded) with SLP (hPa; black contour lines with a 5 hPa interval) at 06 UTC 03 Jan 2017. Colored contour lines show areas of CAA (blue) and WAA (orange).

3.3 Precipitation Patterns

As shown in Figs. 7c and 7d, the observed precipitation does not correspond well with the areas of CAA or WAA. It rather coincides with the fronts of the cyclone where convergence of air masses occurs and the vertical winds are strongest (Fig. 6d). Furthermore only little P occurs in the CAA area behind the cold front, whereas the warm sector exhibits areas of strong P. During the case study, P does not develop continuously. At the start of the case study, quite strong P occurs in the warm sector of the still rather small low pressure system. As the cyclone develops, the amount of total P decreases until the formation of the cold front, when a strong increase in P along the front is visible.

For the characterization of CAA and WAA it is also interesting to see how the precipitation can be divided in CP and LSP. In the early stage of the cyclone, P is primarily LSP. This relation is sustained also after the front formation. However along the front, some

CP can be observed (Fig. 7c) as strong updrafts are generated in this area (Fig. 6d). In the warm sector, P occurs mainly as LSP as it forms due to large-scale uplift of air masses. Further analysis of the precipitation budget during CAA and WAA events is performed in Chapter 4.4.

3.4 History and Future of CAA and WAA Air Masses

The trajectory analysis for the case study shows that the air mass which is ending up in the area of strong WAA originates mainly from lower to mid-levels (Figs. 8a, 9). Between -140h and -70h prior to the WAA event, the air parcels descend strongly in height with an anticyclonic rotation forced by the large anticyclone to the southeast of South Africa (Fig. 8a). During their subsidence, the air parcels experience a strong increase in temperature, partially due to adiabatic warming. At the same time, q increases by a factor of 4 (Fig. 10a). During the two days before the event, the warm and moist air remains very close to the surface and the RH increases again (Fig. 10b). During the WAA event, the air parcels lose q rapidly and at the same time show a massive gain in LWC due to cloud formation and precipitation (Fig. 10c). 48h after the event, the LWC decreases again as well as the RH, although some of the air parcels are maintaining their high RH. The temperature of the WAA air mass decreases in the two days following the event on average about 15°C as the air parcels are lifted into a region between 800 and 850hPa.

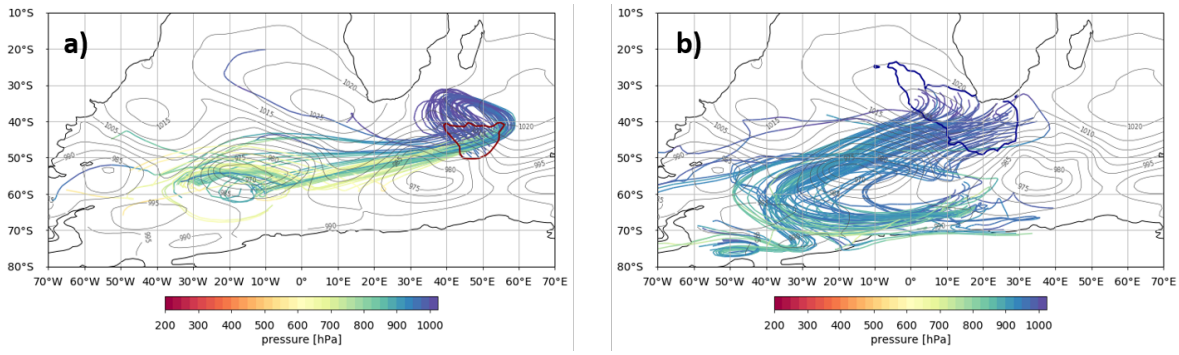

Figure 8: 10-day backward trajectories initialized at 06 UTC 03 Jan 2017 from an area of (a) strong WAA (red contour line) and (b) strong CAA (blue contour line), color-coded according to the pressure along the trajectories (hPa). Black contour lines show SLP in hPa (with a 5 hPa interval) at 06 UTC 03 Jan 2017.

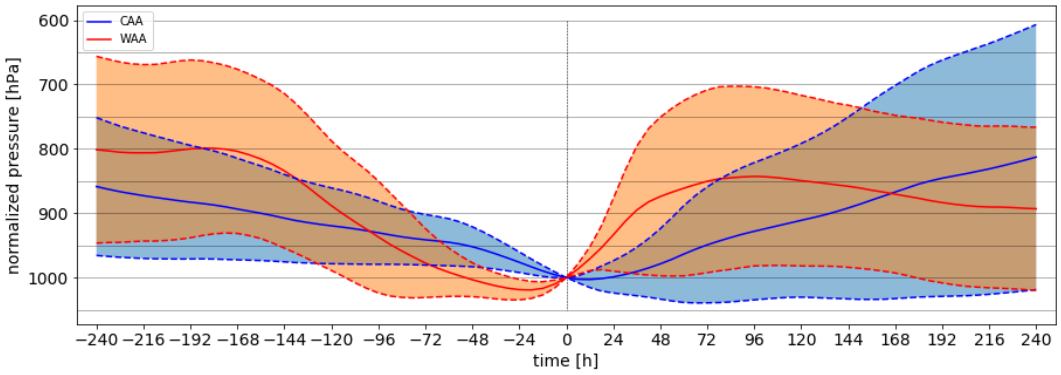

Figure 9: Mean normalized pressure (hPa) conditions along trajectories, reaching the surface during WAA (red line) and CAA (blue line) at time=0h (vertical line) including the standard deviation (colored areas). Trajectories calculated for 240 hours prior and 240 hours after the event at time=0h in 6-hourly steps between 18 UTC 01 Jan 2017 and 06 UTC 04 Jan 2017.

The air mass which is leading to strong CAA originates from the lower levels close to the Antarctic ice sheet and transport cold and dry polar air towards the mid-latitudes (Figs. 8b, 9). Compared to the WAA air mass, the air parcels undergo only minor subsidence. Shortly after the CAA event they even sink a bit more, before they ascend again slowly. Prior to the event, the air mass does not experience such a strong moistening as it is the case for the WAA air mass (Fig. 10a). As the temperature of the air parcels is increasing during the two days prior to the CAA event, the RH drops to values between 60% and 75% (Fig. 10b). The liquid water content of the CAA air mass decreases to very low values. During the CAA event and the following 48 hours, q continues to rise and the RH increases again due to strong evaporation. Interestingly, after the CAA event, the air parcels are mostly keeping their high moisture content over the next few days. An increase in LWC after 24h indicates condensation and cloud formation.

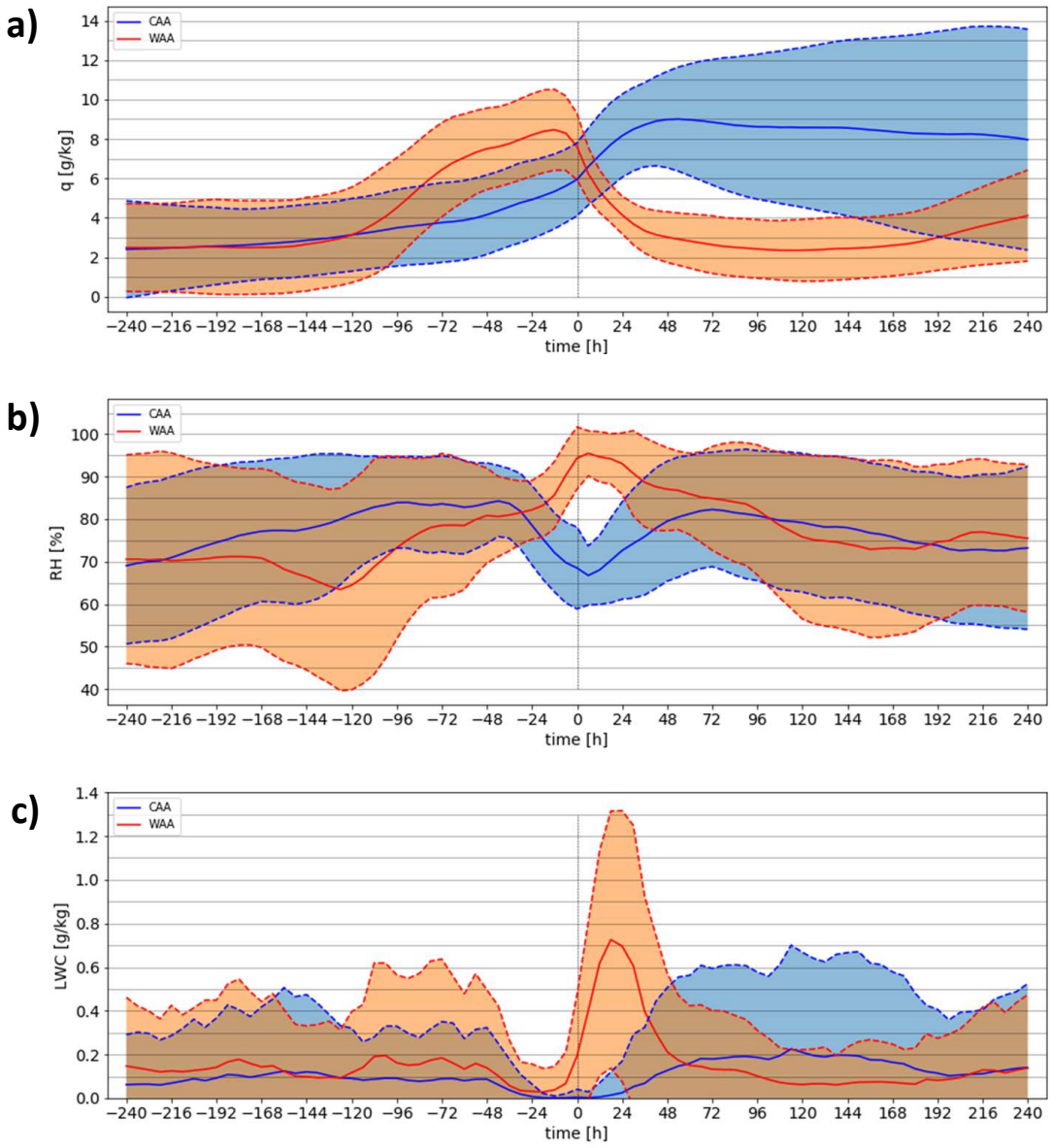

Figure 10: Mean (a) q (g/kg), (b) RH (%) and (c) LWC (g/kg) conditions along trajectories reaching the surface during WAA (red line) and CAA (blue line) at time=0h (vertical line) including the standard deviation (colored areas). Trajectories calculated for 240 hours prior and 240 hours after the event at time=0h in 6-hourly steps between 18 UTC 01 Jan 2017 and 06 UTC 04 Jan 2017.

4 Climatology

The performed case study revealed distinct patterns of the surface fluxes during CAA and WAA in the South Indian Ocean. To get a better understanding of the regional distribution and impact of CAA and WAA events on a longer timescale, a climatology of CAA, ZAA and WAA is calculated for this region. First, the seasonal frequency and the spatial distribution of the different advection types is analyzed. Then, climatological mean values for air-sea interactions during CAA and WAA are calculated and interpreted, using the CAA and WAA frequencies as a reference. Finally, the influence of CAA and WAA on the hydrological budget is assessed quantitatively.

4.1 Temperature Gradient T_{10m}-SST

For the calculation of the climatology, the objective identification scheme for CAA and WAA (section 2.2.1) is applied to ERA-Interim reanalysis data for the period 1979-2016. The temperature gradient T_{10m}-SST which is used in the identification scheme is calculated globally and in the target region. The distribution of T_{10m}-SST is shown with histograms, smoothed with a Kernel Density Estimation, for these regions (Fig. 11). The region of the South Indian Ocean shows distinct features in the distribution during summer (DJF) and winter (JJA) (Fig. 11a).

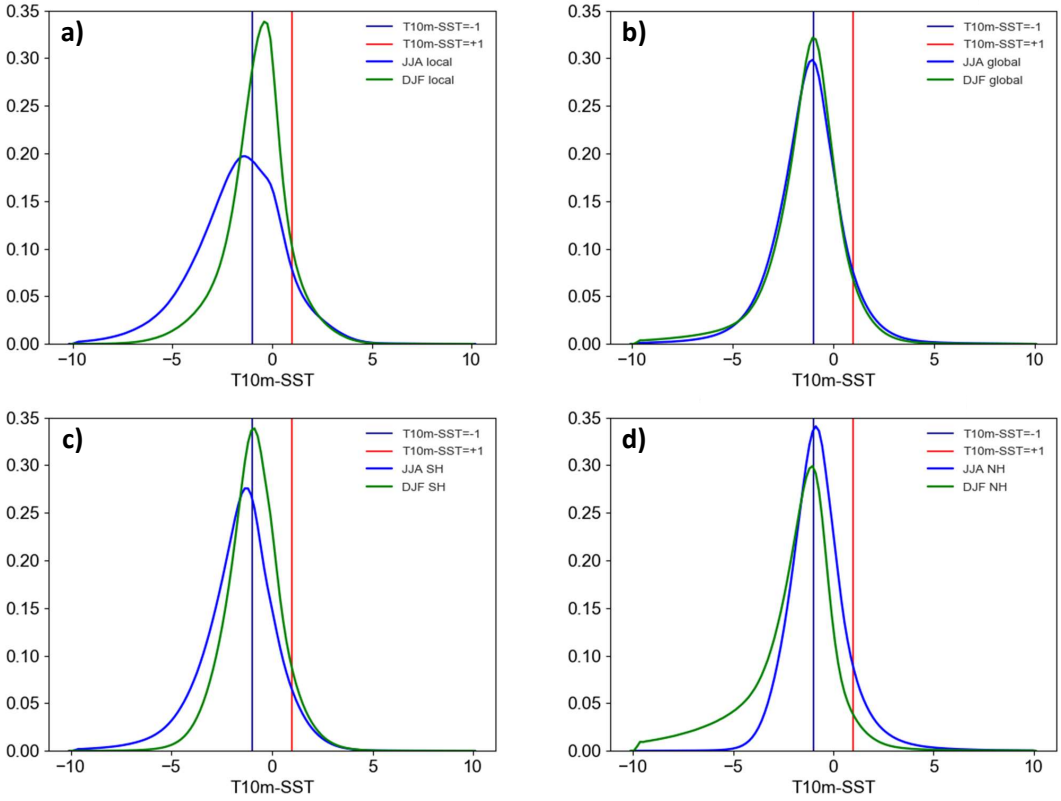

Figure 11: Distribution of $T_{10\mathrm{m}}$-SST (K) during DJF (green line) and JJA (blue line) (a) in the study area, (b) globally, (c) on the Southern Hemisphere and (d) on the Northern Hemisphere. Areas of CAA, ZAA and WAA are separated by vertical lines.

In winter, the distribution of $T_{10\mathrm{m}}$-SST in the study area is much broader and shows a maximum around -2K which means that most often the grid points in this area experience CAA. The summer maximum however is located in the region of ZAA and less CAA occurs. To categorize these distributions in a global context, Fig. 11b shows the global range of $T_{10\mathrm{m}}$-SST. A small shift towards more CAA situations in the study region is visible during JJA which is probably due to the larger oceanic area on the Southern Hemisphere where CAA is dominant during these months (Fig. 11c). In general, the global mean value of $T_{10\mathrm{m}}$-SST lies around -1K which points out a clear asymmetry between CAA and WAA. This asymmetry can be mainly explained with the large heat capacity of the ocean compared to fast radiative cooling processes in the atmosphere. As Figs. 11c and 11d show, there is a general shift towards CAA events during winter.

4.2 Advection Frequency of CAA and WAA

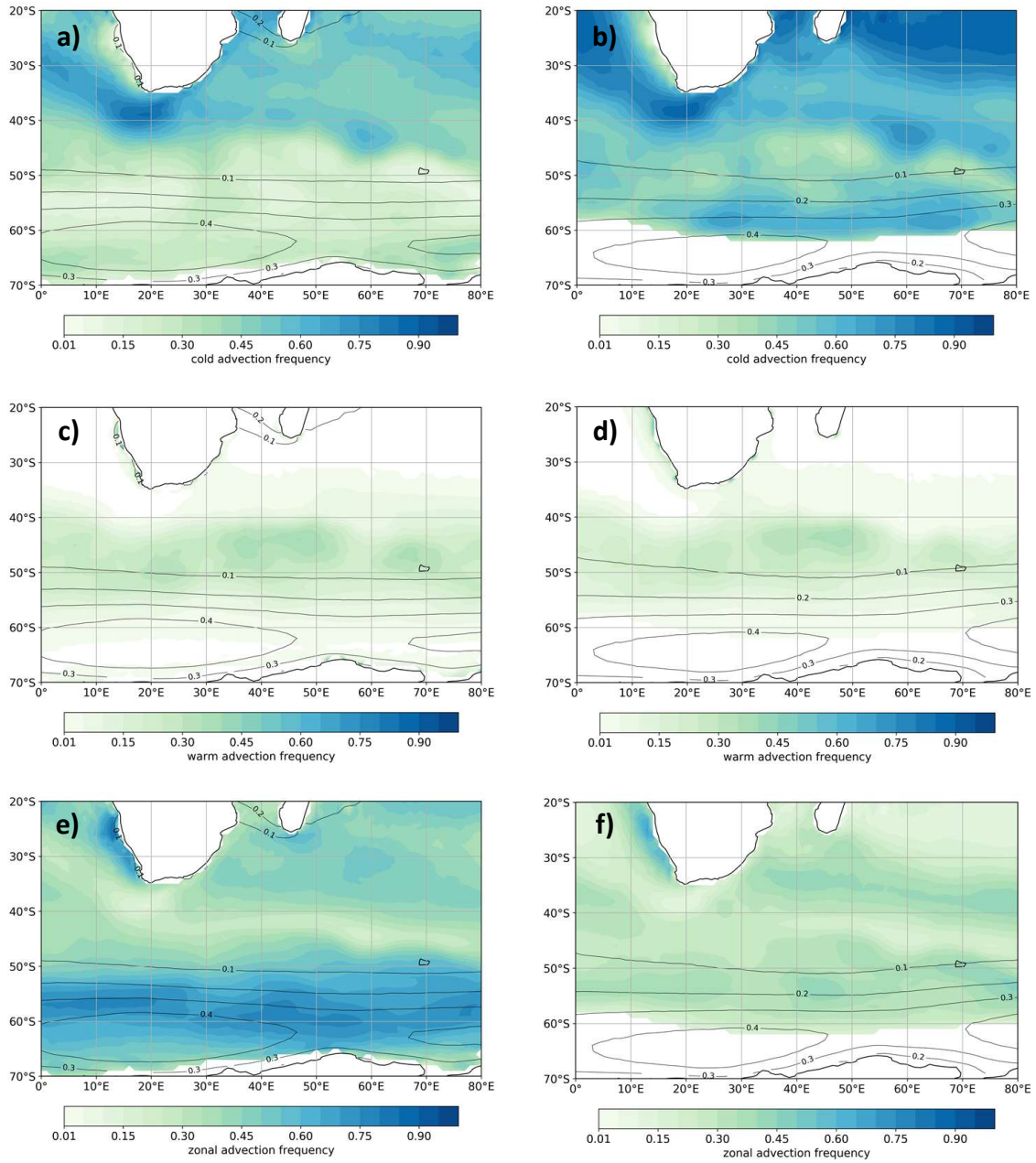

Figure 12: Frequency of CAA events (shaded) during (a) DJF, (b) JJA, frequency of WAA events during (c) DJF, (d) JJA, frequency of ZAA events during (e) DJF, (f) JJA. Black contour lines show the cyclone frequency (Wernli and Schwierz, 2006) during (a,c,e) DJF and (b,d,f) JJA.

Figure 12 shows the frequency of CAA, WAA and ZAA events during austral summer (DJF) and austral winter (JJA). The sea-ice extent around Antarctica is flagged as white area around the continent. Again, the asymmetry between the number of CAA and WAA events is clearly visible as well as the more frequent occurrence of CAA events in winter. In general, CAA occurs more frequently in the subtropics in a band between 35°S and 45°S, whereas WAA occurs most frequently in the mid latitudes between 40° and 50°S.

A "hot spot" of strong CAA during the whole year is located in the region of the warm Agulhas current west of the African continent, which favours CAA. The CAA in the subtropics is much more enhanced in winter, possibly due to more frequent dry air intrusions (Raveh-Rubin, 2017). During winter, an additional band of enhanced CAA is visible between 50° and 60°S (Fig. 12b) along the sea ice edge. Around the Antarctic continent, advection of very cold air masses from the continent can lead to CAA events. Particularly during wintertime, when the air is radiatively cooled compared to the ocean which remains warmer, cold air outbreaks along the Antarctic coast occur frequently (Bracegirdle and Kolstad, 2010). An additional feature during winter is the extent of the sea-ice around Antarctica. Cold air from the antarctic interior can then be transported over the sea-ice to lower latitudes with higher SST compared to the summer months, when the sea-ice edge is further south. In general, CAA occurs frequently in regions with different weather regimes, which becomes more clear when looking at the mean horizontal wind speed (Fig. 13). The mean wind speed during CAA appears to be lower when compared to WAA events although large areas of CAA occur behind cold fronts. However, CAA does also occur frequently in areas of high-pressure systems, where the horizontal wind speed is low compared to the low-pressure systems to the South. The seasonal difference in the mean horizontal wind speed during CAA occurs due to the increase in cyclone frequency and intensity in winter.

WAA, which occurs close to fronts, can be related to high horizontal wind speeds (Figs. 13b, d). The seasonality in frequency is less pronounced for areas of WAA (Figs. 12c, d). The frequency of WAA events is slightly larger during summer (Fig. 12c). Single spots of slightly higher WAA frequency along the west coast of South Africa as well as along Antarctica indicate that in these regions interactions with continental air masses are important. The stronger occurrence of WAA between 40° and 55°S corresponds to an area with lower CAA frequencies, as this is the region where most of the warm sectors pass. The frequency of warm sectors and associated fronts shows only a small seasonality.

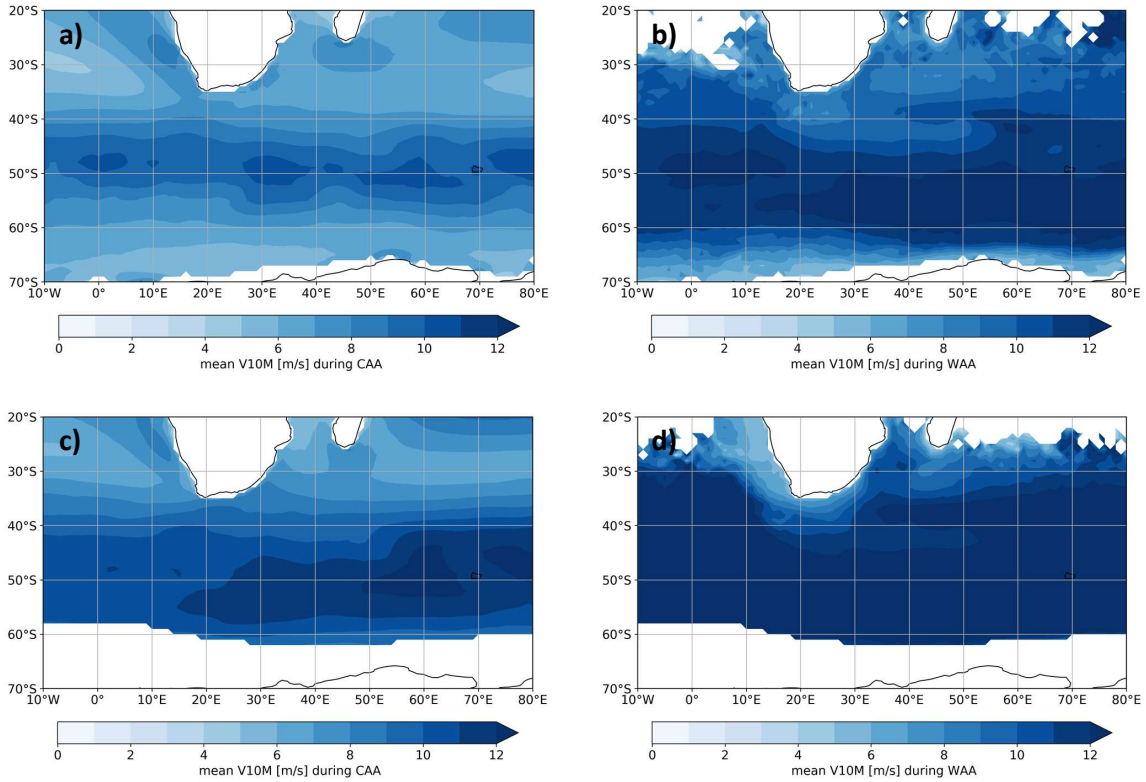

Figure 13: Mean horizontal wind speed at 10m (m/s; shaded) during (a) CAA in DJF, (b) WAA in DJF, (c) CAA in JJA, (d) WAA in JJA.

In general, more areas of CAA than WAA are observed, which can be explained by the large heat capacity of the ocean in comparison to the faster radiative cooling of the atmosphere. Associated with cyclones the areas of CAA are often also larger, as the cyclonic cold sector usually is larger than the warm sector. It is also important to compare the temperature gradient with the actual SST to better understand the spatial patterns of frequent occurrence of CAA and WAA respectively. Figure 14 shows the mean climatological SST during summer and winter, respectively. One dominant feature is the Agulhas current to the southeast of South Africa, where relatively warm ocean water is transported all year long to the Cape of Good Hope, a region of frequent CAA. Further does the SST show a strong latitudinal gradient between 35°S and 50°S which coincides with the shift of high CAA frequency between 30°S and 40°S towards a region of high WAA frequency between 40°S and 50°S. The higher latitudes show a relatively consistent mean SST close to 0°C. As air temperatures in this region are usually cooler, especially when the air originates above the Antarctic ice shield, CAA is more frequent in this region. The further the sea-ice is extended to mid-latitudes in winter, the stronger pronounced is this effect.

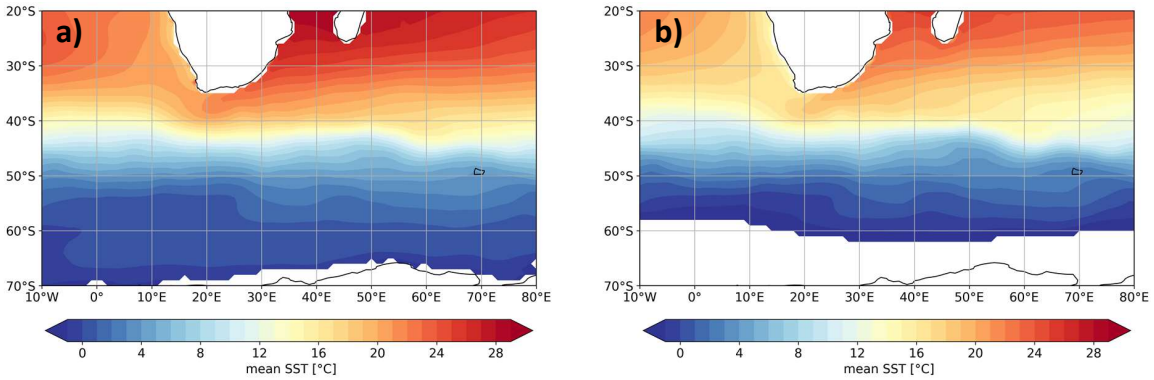

Figure 14: Mean SST (°C; shaded) between 1979 and 2016 during (a) DJF and (b) JJA.

The cyclone frequency, which is shown in Fig. 12, is similar throughout the seasons in the South Indian Ocean. During summer, the highest cyclone frequency values are observed over a slightly larger area than during winter. In the area of maximum cyclone frequency, neither high CAA nor high WAA frequencies can be observed. Due to the dominating strong zonal wind in these areas only weak temperature advection occurs and ZAA is dominating (Figs. 12e, f). A possible explanation for this phenomenon is low-level convergence of northern and southern air masses, which occurs in cyclones. The air temperature of the mixed air masses in the center of the cyclone is similar to the SST and thus CAA and WAA occur less frequently.

4.3 Air-Sea Interactions and Synoptic Environments Associated with CAA and WAA

4.3.1 Evaporation

For the variables introduced in chapter 3, composites are calculated for the whole duration of the climatology. Figure 15 shows the composite for evaporation. During CAA events, the maximum evaporation occurs close to the coast, in the region of the warm ocean currents. During winter months, the values for E are larger which coincides with the increased CAA frequency and the stronger air-sea humidity gradients. Maximum E up to 10 mm/6h can occur in winter. In the region of the storm track, the E values during CAA are strongly reduced in summer coinciding with reduced CAA frequency (Fig. 12a) and larger in winter which is again corresponding to the higher CAA frequency (Fig. 12b). In addition, the stronger winds during wintertime (Fig. 13) combined with the advection of colder and drier air than in summer induce stronger surface fluxes.

For the most part, the mean E during WAA events is slightly negative, especially in the regions with the highest WAA frequency. These negative E values indicate the

dominance of dew deposition. Maximum D values of 2 mm/6h can be reached. These values occur in a band between 40° and 60°S, which matches the high frequency of WAA in this area shown in section 4.2. In the subtropics, relatively high values of E up to 4 mm/6h can be observed also during WAA events. These have to be considered with caution, as in this region the frequency of WAA events is rather low. A possible mechanism inducing the high E values can be the advection of dry air from the continent or on the rear side of cyclones that can induce evaporation even in WAA areas. The occurrence of anticyclones in this region can additionally cause the subsidence of dry air. Similar to the WAA frequency, the SLHF during WAA does not show a strong seasonality which supports the assumption that it is strongly linked to the type of advection. During the summer months, D can be observed further north than during winter. Furthermore reduced values of E can be observed in summer, as the atmosphere is in general warmer and moister which leads to a reduction in E. This is valid for both advection types.

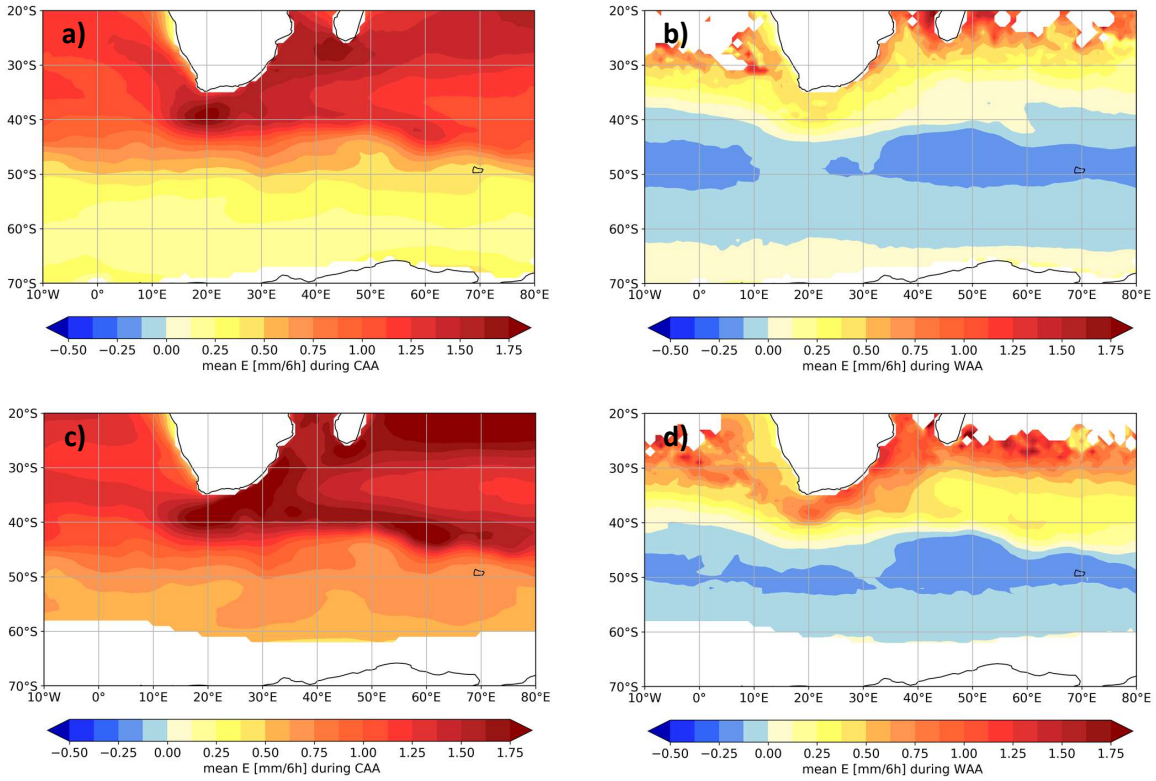

Figure 15: Mean E and D (mm/6h; shaded, positive values show E, negative values show D) during (a) CAA in DJF, (b) WAA in DJF, (c) CAA in JJA, (d) WAA in JJA.

4.3.2 Surface Sensible Heat Flux

The mean values for SSHF can be seen in Fig. 16. The seasonality for CAA events is apparent, and the distribution of SSHF corresponds better to the frequency of CAA (Figs. 12a, b) than E (Fig. 15a,c), particularly in winter. Whereas the SSHF displays mainly the temperature gradient and matches thus very well with the advection frequencies, E is also strongly dependent on the RH_{SST} (Figs. 17a, c). Close to the sea-ice edge, cold air induces strong CAA and SSHF in winter, but as the air is that cold, it can not hold as much moisture as in lower latitudes, which restricts the amount of E. During winter, maximum SSHF values up to -550 W/m^2 occur in the mid latitudes (Fig. 16c) and close to the Antarctic continent. In the subtropics, however, SSHF decreases.

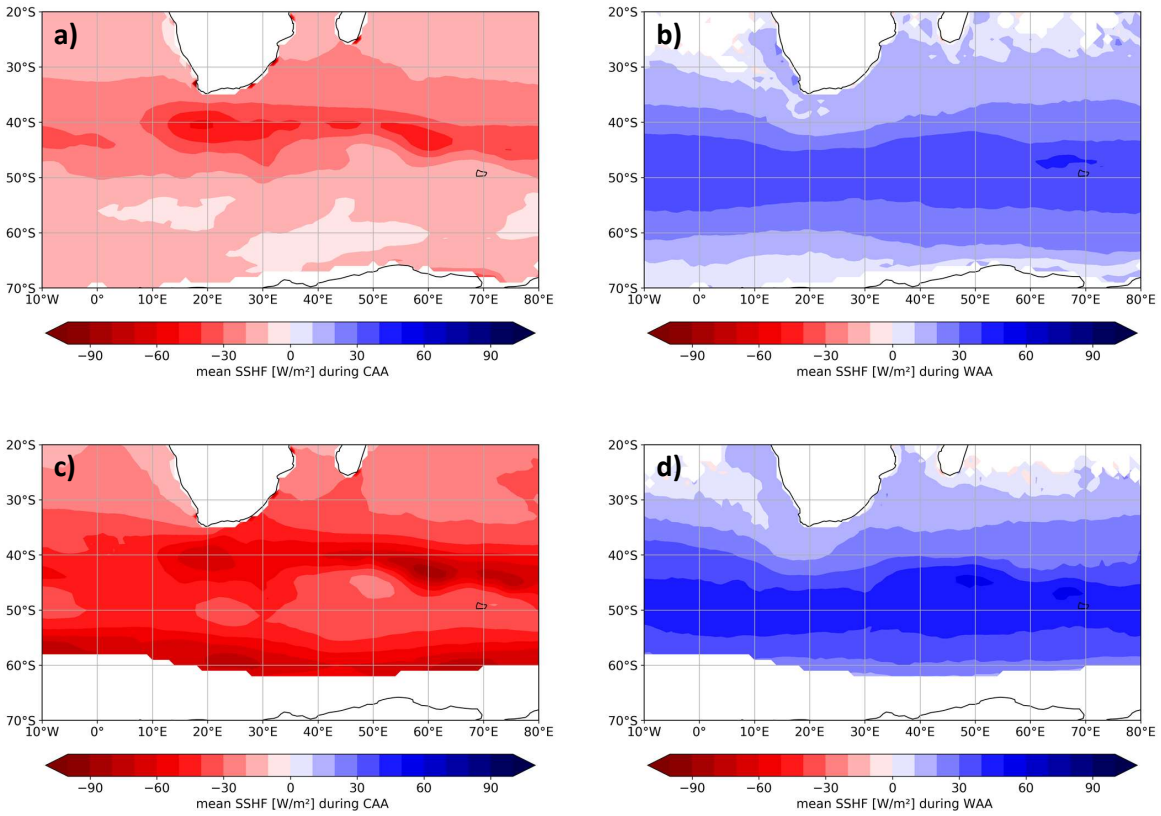

Figure 16: Mean SSHF (W/m^2; shaded) during (a) CAA in DJF, (b) WAA in DJF, (c) CAA in JJA, (d) WAA in JJA.

The mean SSHF during WAA events is stronger during winter, reaching up to 230 W/m^2 and slightly weaker during summer in contrast to the WAA frequency. However the distribution of SSHF does not seem to have a strong seasonality regarding WAA events.

During winter, when the ocean acts as a "heat container", sensible heat fluxes into the relatively colder atmosphere are enhanced. The simultaneous increase in SSHF directed

into the ocean during WAA events can be explained with a lower SST during winter, which enhances the fluxes during WAA. It is also evident that the asymmetry in the strength of E and D during CAA and WAA (Fig. 15) does not occur for the sensible heat fluxes, as they only depend on the actual temperature difference between ocean and atmosphere. Latent heat fluxes however are also dependent on the humidity gradient, which is mostly directed into the ocean and favours evaporation into the atmosphere.

4.3.3 Relative Humidity

The relative humidity with respect to the SST, RH_{SST}, is next to the horizontal wind speed an important measure for the exchange between atmosphere and ocean, as it is an important driver for E and D. The seasonal mean values during CAA and WAA are shown in Fig. 17. As already emphasized in section 3.2, regions of CAA feature on average very low values of RH_{SST} whereas during WAA the values are much more enhanced and often saturation is reached. During winter, when the sea-ice extent reaches the mid latitudes, dry cold air form the Antarctic continent results in even drier conditions during CAA as in the summer months. The areas of high WAA frequency feature the highest RH_{SST} values. However, RH_{SST} can be reduced during WAA in the subtropics when dry air is advected, especially in winter when dry air intrusions are enhanced in this region (Raveh-Rubin, 2017). The RH_{SST} patterns can explain the surface latent heat fluxes in form of E and D during CAA and WAA (section 4.3.1) for a great part. Whereas low RH_{SST} enhances E, very high RH_{SST} values favour D.

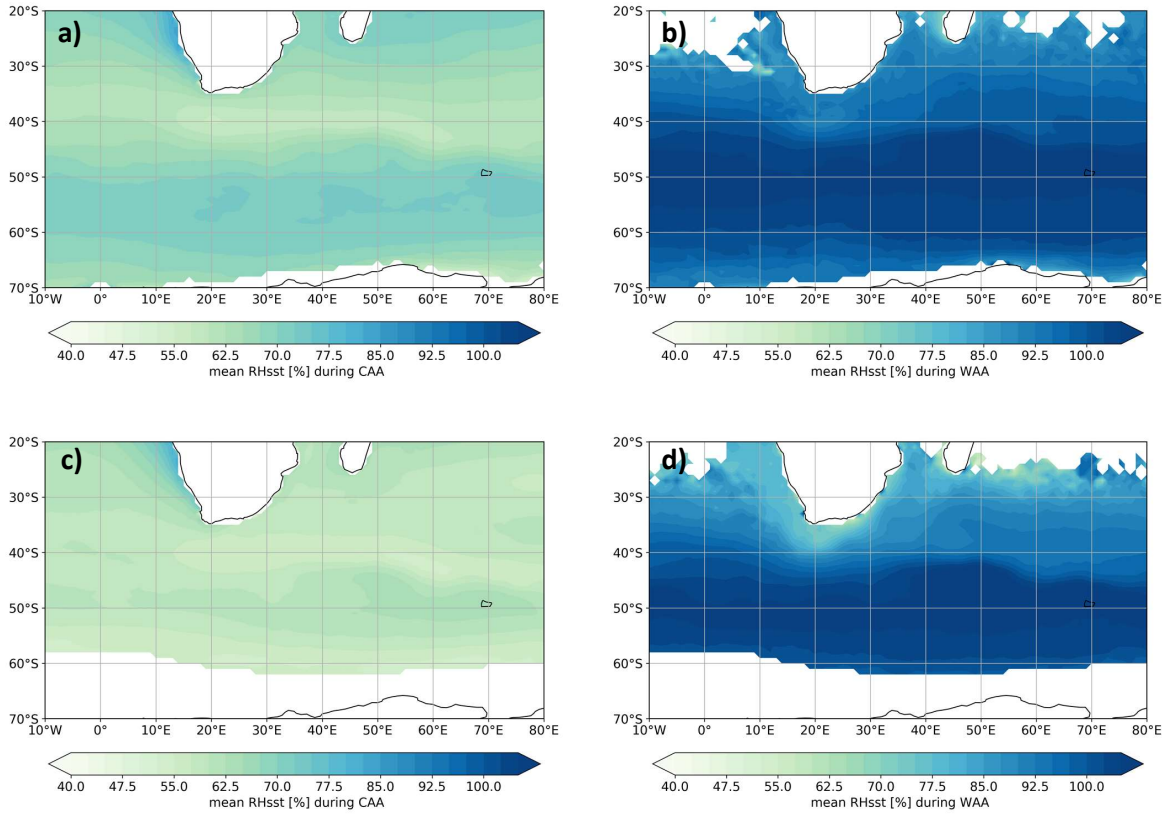

Figure 17: Mean RH_{SST} (%; shaded) during (a) CAA in DJF, (b) WAA in DJF, (c) CAA in JJA, (d) WAA in JJA.

4.3.4 Precipitation Patterns

As already mentioned in section 3.3, most of the precipitation in general coincides with the fronts of the cyclones. The highest intensity in precipitation can be found during WAA as LSP (Fig. 18a), where 6-hourly maxima of 80 mm can be reached mainly in the southeastern part of the study region. This type of precipitation typically occurs in the warm sector of the cyclones ahead of and along the cold front. (Papritz et al., 2014) could show that during winter precipitation related to cyclones and fronts intensifies, which coincides with the general enhancement of LSP in this climatology. CP occurs significantly less frequent during WAA and mostly in the subtropics, where convection occurs (Fig. 18b). In summer, strong CP can be observed in these regions due to the increased SST which reduces the boundary layer stability and thus induces strong updrafts.

During CAA, the precipitation intensity is much lower than during WAA, as these are often regions of strong evaporation and only their proximity to fronts causes precipitation. Thus, LSP during CAA occurs mainly in the region of the storm track, whereas in the subtropics CP can coincide with CAA especially during summer (for further

composites see Fig. A.1).

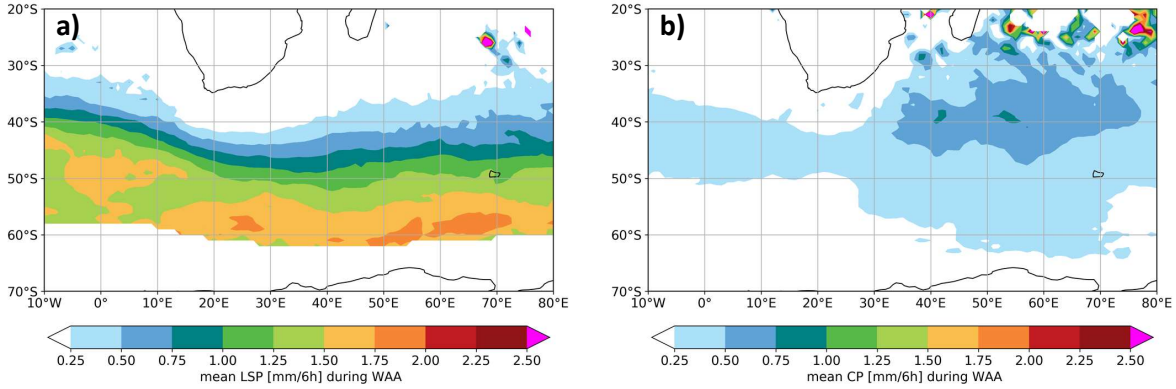

Figure 18: Mean (a) LSP (mm/6h; shaded) during WAA in JJA and (b) CP (mm/6h; shaded) during WAA in DJF.

4.4 Relevance of CAA and WAA for the Hydrological Budget

To further investigate the influence of CAA and WAA on the hydrological cycle, a hydrological budget for the study area is calculated. Figure 19 shows a schematic representation of the freshwater fluxes CP, LSP, E and D, which does not necessarily consider the scale of CP and LSP in correct proportions. For each of the variables, the total flux into the ocean and the atmosphere, respectively, is calculated in km^3 per season. The data at each grid point is weighted according to the area represented by the grid point. Table 1 displays the proportional share of CAA, ZAA and WAA regions for the different freshwater fluxes.

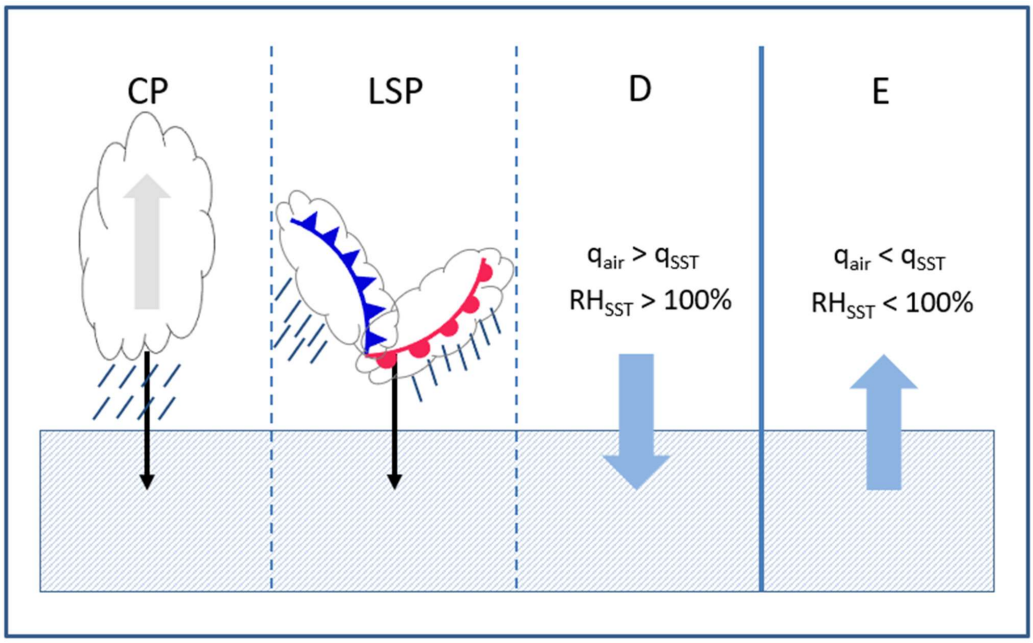

Figure 19: Schematic representation of the freshwater fluxes CP, LSP, D and E.

The yearly ratio of CP to LSP in this region is 43:57. This ratio varies during the year and ranges between 47:53 in winter and 41:59 in summer (Fig. 20). In winter, more than 60% of the CP falls in areas of CAA. In summer it is only about 45%. A similar but less pronounced behaviour can be found for LSP. This pattern can be explained by a higher frequency of strong CAA during winter (section 4.2). In general, a larger share of CP and LSP can be explained by CAA than WAA, which seems to contradict the results from section 4.3.4. However, the asymmetry in advection frequency has to be considered, as CAA occurs more often and covers larger areas and thus the accumulated amount of precipitation in these areas is larger.

The evaporative heat flux is subdivided into E which corresponds to a latent heat flux into the atmosphere and D which corresponds to a latent heat flux into the ocean in the form of dew formation. As the atmosphere is mostly subsaturated with respect to the sea surface, there is a clear ratio of 98:2 of E compared to D. Figure 20 shows a strong seasonality in the amount of E, which is due to the seasonal difference in the CAA frequency. E is dominated by areas of strong CAA. In general, the more negative the temperature gradient T10m-SST, the larger E. The dew formation is on the contrary dominated by strong WAA events which account for more than 60%. This is consistent with the observations in RH_{SST} indicating generally supersaturated air with respect to the sea surface during WAA.

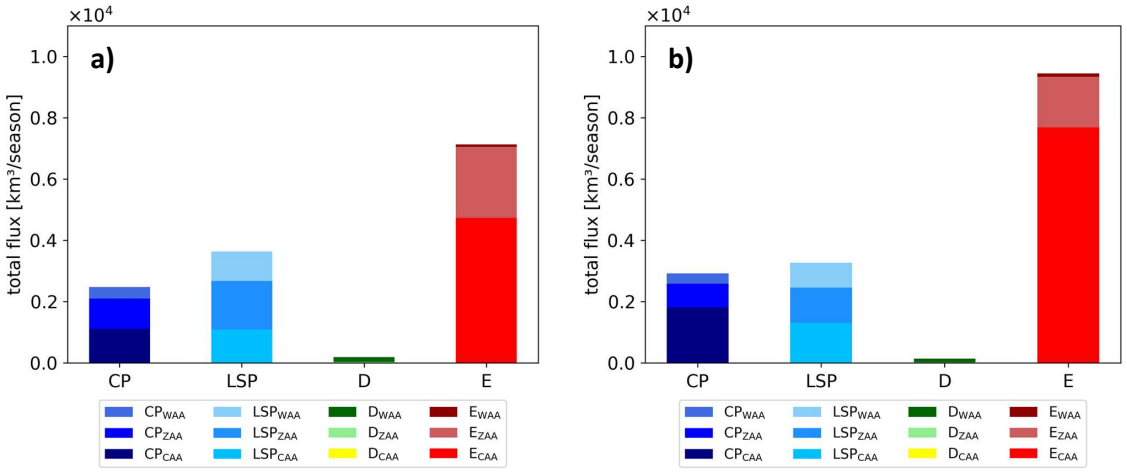

Figure 20: Total flux for CP, LSP, D and E in km^3/season accumulated for (a) DJF and (b) JJA. Different colors in one bar refer to the presence of CAA (upper part), ZAA (middle part) or WAA (lower part) at the grid point.

Table 1: Proportional share of the different advection types for the total CP, LSP, D and E in the study area during DJF (red) and JJA (blue), from ECMWF reanalysis data between 1979-2016. For yearly mean values see Table A.1.

variables	**CAA**	**WAA**	**ZAA**
CP	45%/62%	15%/12%	40%/26%
LSP	30%/40%	26%/25%	44%/35%
D	0%/1%	87%/89%	13%/10%
E	66%/81%	1%/1%	33%/18%

5 Isotope Analysis

In this last part of the thesis, measurements of δ^{18}O and δD in monthly accumulated precipitation on MI are analyzed. First, precipitation on MI is characterized by its synoptic setting and the moisture sources, using backward trajectories and applying a moisture source diagnostic. Second, the SWI measurements in the final P on MI are interpreted with respect to the advection regimes, utilizing the introduced MAI.

5.1 Synoptic Environment and Moisture Source

Figure 21 shows the difference between the mean pressure along backward trajectories and the final pressure at the arrival of the air parcels that lead to precipitation on MI. The trajectories are sorted into trajectories arriving within or above the planetary boundary layer, and they are further divided according to the advection regimes on their arrival. 12% of the trajectories arrive within the PBL, thereof 15% during a WAA event and 53% during CAA. During CAA the PBL is higher than during WAA, as expected due to mixing processes and turbulence resulting from enhanced convection during CAA. The remaining 88% of the trajectories arrive above the PBL, with 35% during CAA and 32% during WAA conditions at the surface. It is evident that CAA air masses tend to undergo subsidence before the event whereas the air parcels in a WAA event tend to ascend 1-2 days prior to arrival, which is representative for the air streams within the cold and warm sector, respectively. As shown in section 3.1, WAA mostly happens during the passage of a warm sector, where warm air is lifted above cooler air. The CAA occurs however after the passage of the cold front, when colder, denser air is subsiding. For ZAA, the temperature gradient T_{10m}-SST is less distinct, thus the air masses show no clear trend of ascending or descending above the PBL. Within the PBL, air masses tend to descend for ZAA, too.

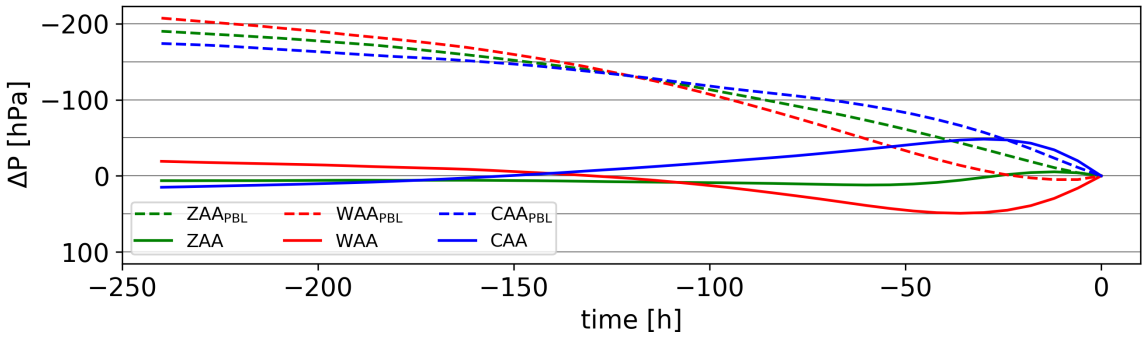

Figure 21: Mean difference between pressure along 10-day backward trajectories and final pressure at MI [hPa] with trajectories starting from MI at 40 different vertical levels during WAA, ZAA and CAA. Dashed lines show trajectories in the PBL, solid lines show trajectories above the PBL. Total number of trajectories in PBL: 27221 and above PBL: 192498.

The region of the moisture source for precipitation on MI is calculated using the moisture source diagnostic tool by Sodemann et al. (2008). Seasonal means for summer and winter are shown in Fig. 22. The mean moisture uptake occurs mainly to the northwest of the island with its maximum close to the coast of South Africa in the region of the Agulhas warm water current. During winter, when the storm track is enhanced, the moisture originates from more westerly longitudes over the South Atlantic. During summer, an important part of the moisture is advected from the region between MI and Madagaskar.

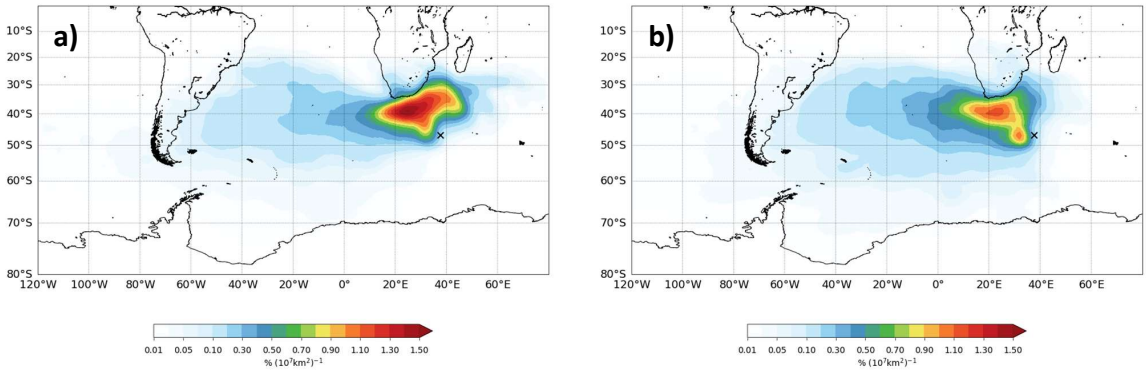

Figure 22: Contour plot for the moisture uptake (% per $10^7 \mathrm{km}^2$; shaded) for P on MI (black cross) for (a) DJF and (b) JJA. See Fig. B.1 for further seasonal moisture source regions during MAM and SON.

Figure 23 shows monthly mean values for the conditions at the moisture source in the form of the mean SST, mean $\mathrm{RH}_{\mathrm{SST}}$ and the MAI. The MAI is continuously negative, indicating high CAA frequency in combination with very low WAA frequencies in the moisture source region. This is consistent with Figs. 12 and 22, as the Agulhas current favors CAA conditions and thus moisture uptake. The seasonal cycle of the MAI can be mostly explained with fluctuations in ZAA frequency and thus reduced CAA frequency, especially during summer (see also Fig. 25). It is coincident with the seasonality of $\mathrm{RH}_{\mathrm{SST}}$, which shows the lowest values during winter. Thus we can expect to find enhanced d in precipitation for the winter months. The SST shows slight seasonal changes with maximum values in autumn and minimum values at the end of winter.

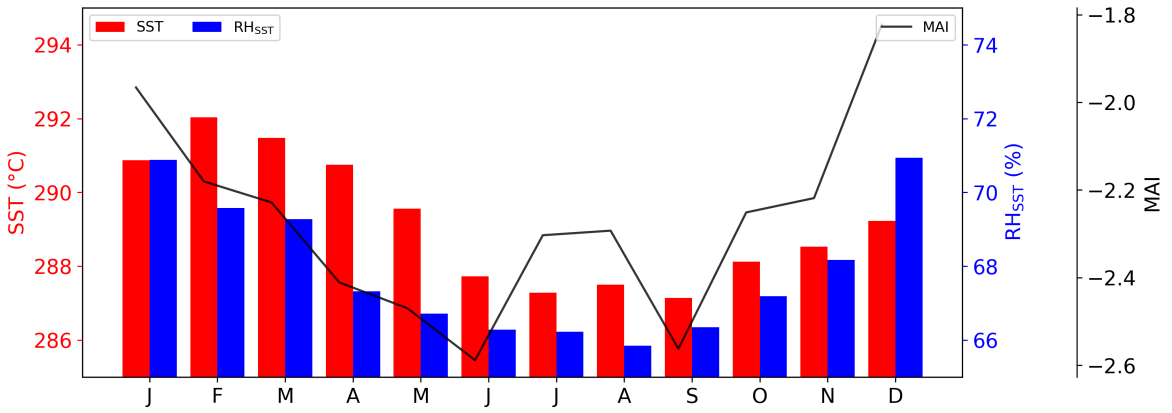

Figure 23: Monthly mean values of SST (°C; red bars), RH_{SST} (%; blue bars) and the MAI (black line) at the moisture source for MI.

5.2 Imprint of the MAI on SWI measurements

Figure 24 shows scatter plots of monthly measurements of $\delta^{18}O$ and δD colored by the MAI on MI (Fig. 24a) and at the moisture source (Fig. 24b). The precipitation on MI tends to be more enriched in SWI when WAA is more frequent and more depleted when CAA dominates. However, there is no clear clustering in the data points which would separate measurements during a high MAI from measurements during a low MAI. At the moisture source, the MAI is strongly negative for all months as shown in Fig. 23. CAA is dominant at the moisture source, which can be explained by the fact that significant moisture uptake is only expected during intermediate to strong E which mainly occurs during CAA whereas D is predominant during WAA (section 4.4).

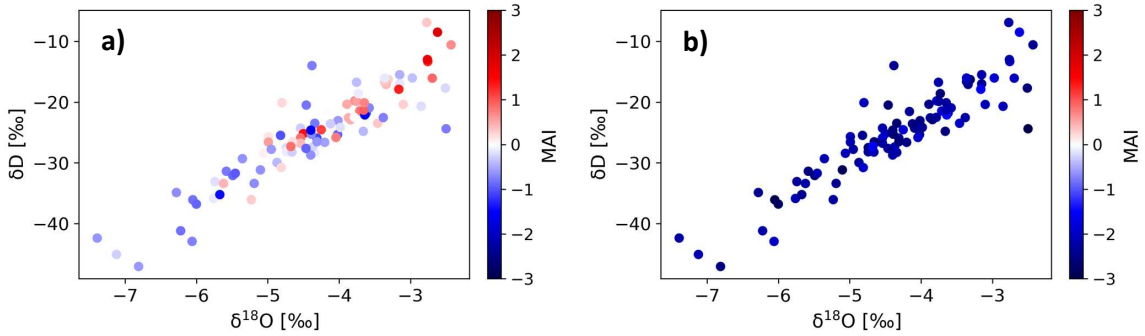

Figure 24: Scatter plot of monthly measurements of $\delta^{18}O$ and δD on MI, colored according to the (a) MAI on MI and (b) MAI at the moisture source.

The MAI reflects the synoptic conditions in the precipitation region on MI as well as at the moisture source. In the region of the moisture source, evaporation (Fig. 15) is strongly enhanced and thus moisture uptake is favored. On MI however, the advection regimes are more balanced and several months show a positive MAI with dominating WAA conditions. In combination with the frequent occurrence of warm sectors, precipitation is favored. However, some months show a pronounced negative MAI during P on MI, as the topography of the island can induce orographically enhanced P, regardless of the WAA frequency.

Table 2: Pearson correlations between moisture source conditions (index s) and conditions at MI (index MI) from all monthly d, δ^{18}O and δD data at the GNIP station Marion Island.

variable/variable	$\boldsymbol{d}$	$\boldsymbol{\delta^{18}O}$	$\boldsymbol{\delta D}$
SST_s	-0.56	0.69	0.69
$RH_{SST,s}$	-0.64	0.72	0.66
$f_{CAA,s}$	0.47	-0.65	-0.62
$f_{WAA,s}$	-0.12	0.44	0.50
MAI_s	-0.29	0.57	0.59
$f_{CAA,MI}$	0.53	-0.80	-0.75
$f_{WAA,MI}$	-0.31	0.77	0.75
MAI_{MI}	-0.47	0.83	0.78

Table 2 shows a positive correlation between the SST and the RH_{SST} at the moisture source with the measured SWI. δ^{18}O and δD tend to be more enriched when higher SST and RH_{SST} occur at the moisture source (Fig. B.3), which is consistent with other studies (Pfahl and Wernli, 2008; Aemisegger, 2018). Similar, lower SST and decreased RH_{SST} at the source lead to a depletion in the SWI measurements. Interestingly, the correlation between the MAI on MI and the SWI seems to be very good, even better than at the moisture source. Partially this correlation can be explained with the large-scale character of particularly CAA areas, which can cover both, MI and the moisture source region. However, processes during the moisture transport such as below cloud evaporation and cloud formation can affect both, the MAI and the SWI composition in the final P. To better understand the link between the MAI and SWI enrichment in P at the same location, these processes will need further investigation.

As a measure for non-equilibrium processes at the ocean surface, d is an important indicator for surface fluxes. Figure 25 shows inter-annual monthly mean d in precipitation on MI combined with the corresponding WAA, ZAA and CAA frequency on MI and at the moisture source, respectively. On MI, CAA shows a pronounced seasonality with its peak frequency during winter (Fig. 25a). This increased occurrence of CAA

in winter can be explained by the latitudinal shift of the storm track which leads to a higher frequency of the passage of cold sectors at MI.

The advection frequencies reflect the location of MI in the storm track region, where CAA shows a pronounced seasonality with its peak frequency during winter (Fig. 25a). WAA occurs fairly frequently due to the continuing passage of warm sectors in this area with a slightly increased frequency during summer. On average, the different advection frequencies are similar but seasonally varying, which emphasizes the interesting location of MI for SWI analysis. The MAI at the moisture source is continuously very negative due to a high CAA frequency and only little WAA at the moisture source (Fig. 25b).

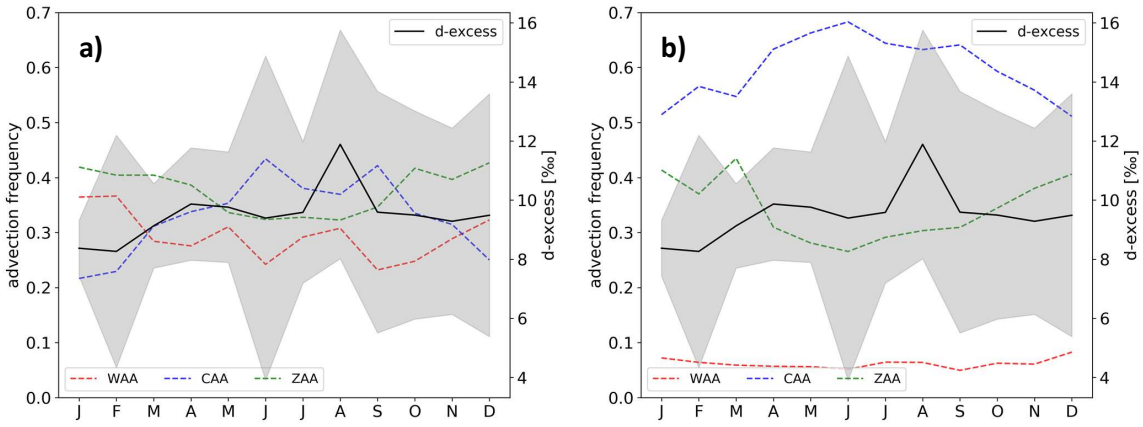

Figure 25: Monthly mean values (black line) and standard deviation (grey shaded) of d on MI and the WAA frequency (red dashed line), ZAA frequency (green dashed line) and CAA frequency (blue dashed line) (a) on MI and (b) at the moisture source.

d shows a seasonal cycle, which correlates with the CAA frequency at the moisture source (Table 2, Fig. 25b), showing a Pearson correlation of 0.47. As shown previously in section 4.3.3, CAA leads to reduced RH_{SST} conditions (Fig. 17). This fits with the larger d values during summer, when the lowest values of RH_{SST} can be observed at the moisture source (Fig. 23). In such conditions, non-equilibrium fractionation is favored resulting in high d values. On MI, d correlates well with the CAA frequency as well, especially during autumn and winter.

In general, d shows only small seasonal variability compared to a large inter-annual variability. Single months show exceptionally high d values, indicating potentially extraordinary non-equilibrium conditions at the moisture source or strong modification during the moisture transport in these months. The high variability of d in the winter and spring months can be partially attributed to changes in the moisture source location. The moisture source is then spread over a larger area, which results in a larger variability of the MAI and thus moisture source conditions (Fig. B.4a). The standard

deviation of the SST and the RH_{SST} in the moisture source region varies between 3.5 °C and 7 %, respectively, in spring and summer compared to 2.8 °C and 5.75 %, respectively, in autumn and early winter (Fig. B.4b).

The SWI measurements in combination with the moisture source diagnostic show the influence of the advection type on the conditions at the moisture source and thus its influence on the SWI composition in P. Strong CAA is the driver of strong moisture uptake as a result of low RH_{SST}, resulting in enhanced non-equilibrium fractionation at the moisture source. These conditions are reflected in the monthly d values.

6 Conclusions and Outlook

Weather systems are an important driver of freshwater fluxes between ocean and atmosphere and thus for the hydrological cycle. Several studies emphasized especially the role of cyclones and fronts for strong air-sea interaction events such as heavy precipitation and strong large-scale ocean evaporation. Especially in the Southern Ocean such events are crucial in determining the ocean stratification and thus formation of sinking water masses. The advection of warm and cold air is associated with the warm and cold sector of cyclones. In this Master's Thesis, the influence of CAA and WAA on freshwater fluxes in the region of the South Indian Ocean has been investigated. In addition, the imprint of CAA and WAA frequency in the SWI composition of precipitation has been analyzed to improve the understanding of moisture sources and transport processes in this region.

In the first part of the thesis, a case study has been performed to examine typical air-sea interactions during CAA and WAA events. The regions of CAA and WAA are dominated by the structure of the cyclone. Strong WAA occurs mainly in the warm sector, whereas the subsiding cold air behind the cold front leads to strong CAA in the cold sector. The interaction in form of sensible and latent heat fluxes between ocean and atmosphere is strongest in these areas, driven by the pronounced temperature gradient $T_{10\mathrm{m}}$-SST and the humidity gradient. Very high $\mathrm{RH}_{\mathrm{SST}}$ values reaching saturation can be observed in areas of strong WAA, favoring dew deposition. In contrast, areas of strong CAA show very low $\mathrm{RH}_{\mathrm{SST}}$ values, inducing strong evaporation. Precipitation occurs mainly as LSP along the fronts of the cyclone and is less influenced by the patterns of CAA and WAA, respectively.

The air reaching the warm sector of the cyclone experienced subsidence in an adjacent anticyclone accompanied by a temperature increase and strong humidification. During the WAA event, cloud formation and precipitation can be observed, leading again to a drying of the air mass. In contrast, the CAA air mass originates from the region of the Antarctic ice shield and transports cold and dry air towards the cold sector. After reaching the surface, a strong moistening of the air parcels can be observed, as the dry air causes extensive evaporation. The strong moisture uptake results in cloud formation along the CAA air mass on the subsequent days.

To better understand the spatial and temporal distribution of CAA and WAA events during different seasons, a climatology of CAA and WAA events in the South Indian Ocean has been calculated. It reveals a strong asymmetry of CAA and WAA frequency in the research area, which is especially pronounced during winter. The ability of the ocean to store heat compared to fast radiative cooling processes in the atmosphere favors the occurrence of CAA events. Especially in the area of the Agulhas warm water current and during winter in the mid-latitudes close to the sea-ice edge, the CAA frequency is enhanced. In addition, subsiding cooler air in anticyclones leads to CAA in

the subtropics. WAA events occur predominantly during the passage of warm sectors in the mid-latitudes. The storm track region shows enhanced ZAA frequency, as low-level convergence of southern and northern air masses possibly reduces $T_{10\mathrm{m}}$-SST. The climatology shows a clear correlation for the occurrence of evaporation, dew formation and surface sensible heat flux with CAA and WAA. The mean SSHF is directed into the atmosphere during CAA and vice versa into the ocean during WAA. The flux intensity is proportional to the CAA and WAA frequency in the respective regions and thus enhanced during winter. E is in all seasons strongly enhanced during CAA, particularly in the region of the Agulhas current. In areas with high WAA frequency, D occurs on average during WAA. However, enhanced E can be observed during WAA conditions in the subtropics, where warm, dry air can be advected from the African continents or in anticyclones, inducing E. The precipitation patterns do not show significant coincidence with WAA or CAA areas. Regions of WAA show higher mean P values, especially as LSP. Precipitation during CAA is lower and mostly caused by frontal systems and convection in the subtropics.

SWI are important tracers for phase-change processes in the atmospheric water cycle and can be used to analyse moisture sources and transport processes. In this study, the imprint of CAA and WAA frequency on SWI composition in precipitation has been investigated, using the defined monthly advection index MAI. SWI measurements in precipitation on MI, an island amidst the research area, have been combined with a moisture source diagnostic, as SWI represent the conditions at the moisture source area as well as transport processes. The mean moisture source of MI is located to the northwest in the region of the Agulhas current with a slight shift towards the Atlantic Ocean during winter. At the moisture source, CAA events are dominating and only little WAA occurs, which favors E and thus the moisture uptake. Low $\mathrm{RH_{SST}}$ during strong CAA combined with the warm SST in the moisture source region enhance non-equilibrium fractionation and result in a high d-excess. Throughout the year, the CAA frequency at the source correlates moderately with the measured d on MI, showing a maximum in winter when the lowest $\mathrm{RH_{SST}}$ values can be observed at the moisture source. A correlation of the MAI on MI with the isotope composition is also apparent, as especially areas of CAA are often large-scale features and it thus is likely that they cover both, the source and the precipitation region. The large variability in d values which is particularly pronounced during spring results from increased variability of the moisture source region and thus the predominant conditions.

This study shows as expected mostly a very good correlation of areas with strong CAA and WAA, respectively, and enhanced air-sea interactions in the form of SSHF, E and D. Further, CAA and WAA frequency is represented in the SWI composition of precipitation, especially does CAA show to have an imprint on d. However, it has to be considered that the applied advection identification scheme uses a very simple approach and does not take into account several parameters. It is based solely on the temperature difference between ocean and atmosphere near the surface, neglecting large-scale

transport mechanisms as well as boundary layer mixing processes. Yet, the interesting results obtained even with such a simple definition underline the ability of this identification procedure to describe atmospheric temperature advection to a great extent. A further extension in the definition of CAA and WAA would hopefully show even clearer results, in particular with regard to the large-scale advection features. Another limitation in this study is the availability of the SWI data on MI. Only one data set is used, in which measurements are not continuously available and if then only as monthly mean values. Although a second data set with daily precipitation measurements has been used to select only reliable data, uncertainties in the precipitation data need to be considered. Further, the MAI is calculated based on the ERA-Interim reanalysis data set. As orographic enhanced P on MI is not resolved in the ERA-Interim data, a bias exists between the reanalysis P data and the station P data which is though relatively consistent throughout the year.

Several aspects of the hydrological cycle in the South Indian Ocean could not be analyzed in more detail in this thesis, which leaves some open questions for further research. A more detailed analysis of transport processes leading to CAA and WAA events will be possible with a more sophisticated advection identification scheme. It will help to better understand the role of advection in the context of cyclones and other weather systems as well as its impact on precipitation. Further research is also needed regarding the effect of the sea-ice extent on CAA and WAA frequency, which has been touched upon only briefly in this study. In the context of global warming and variations in sea-ice extent, a better knowledge on its impact on the hydrological cycle will be crucial. Another interesting research question is how the occurrence of both, CAA and WAA, in the so called "false warm sectors" of cyclones can be explained and which implications arise from this for the freshwater fluxes in a cyclone. To validate the correlations between SWI measurements with CAA and WAA frequency in the Southern Ocean, further measurement stations as well as the analysis of ship-based measurements need to be considered. In combination with moisture source diagnostics, the link between moisture uptake, moisture transport and precipitation in the context of CAA and WAA will be further improved.

Acknowledgements

I acknowledge MeteoSwiss and ECMWF for providing access to the ERA-Interim reanalysis data, the GNIP for providing the isotope data set and the SAWS for providing precipitation data on Marion Island. I am very grateful to Iris Thurnherr and Franziska Aemisegger (ETH Zurich) for valuable discussions, their feedback on the manuscript and technical support. You were always available for my questions and provided new ideas, when I was unsure how to proceed. Further I thankfully acknowledge Natalia Machado Crespo (ETH Zurich and University São Paulo) for inspiring discussions and comments on this Master's Thesis. Thanks for providing your knowledge about the Southern Hemisphere. Finally, I would like to thank the group of Atmospheric Dynamics (ETH Zurich) for their valuable feedback on several aspects of the thesis and their encouragement.

References

Aemisegger, F. (2018). On the link between the North Atlantic storm track and precipitation deuterium excess in Reykjavik. *Atmos. Sci. Lett.*, 19:e865.

Aemisegger, F. and Papritz, L. (2018). A climatology of strong large-scale ocean evaporation events. Part I: identification, global distribution, and associated climate conditions. *J. Clim.*, 31:7287–7312.

Aemisegger, F. and Sjolte, J. (2018). A climatology of strong large-scale ocean evaporation events. Part II: Relevance for the deuterium excess signature of the evaporation flux. *J. Clim.*, 31:7313–7336.

Aemisegger, F., Spiegel, J. K., Pfahl, S., Sodemann, H., Eugster, W., and Wernli, H. (2015). Isotope meteorology of cold front passages: A case study combining observations and modeling. *Geophys. Res. Lett.*, 42:5652–5660.

Araguás-Araguás, L., Froehlich, K., and Rozanski, K. (2000). Deuterium and Oxygen-18 isotope composition of precipitation and atmospheric moisture. *Hydrol. Processes*, 14:1341–1355.

Bracegirdle, T. J. and Kolstad, E. W. (2010). Climatology and variability of Southern Hemisphere marine cold-air outbreaks. *Tellus, Ser. A*, 62A:202–208.

Dee, D. P., Uppala, S. M., Simmons, A. J., Berrisford, P., Poli, P., Kobayashi, S., Andrae, U., Balmaseda, M. A., Balsamo, G., Bauer, P., Bechtold, P., Beljaars, A. C., van de Berg, L., Bidlot, J., Bormann, N., Delsol, C., Dragani, R., Fuentes, M., Geer, A. J., Haimberger, L., Healy, S. B., Hersbach, H., Hólm, E. V., Isaksen, L., Kållberg, P., Köhler, M., Matricardi, M., Mcnally, A. P., Monge-Sanz, B. M., Morcrette, J. J., Park, B. K., Peubey, C., de Rosnay, P., Tavolato, C., Thépaut, J. N., and Vitart, F. (2011). The ERA-Interim reanalysis: Configuration and performance of the data assimilation system. *Q. J. R. Meteorolog. Soc.*, 137:553–597.

Dütsch, M., Pfahl, S., and Wernli, H. (2016). Drivers of δ^2H variations in an idealized extratropical cyclone. *Geophys. Res. Lett.*, 43:5401–5408.

Gedzelman, S. D. and Lawrence, J. R. (1990). The isotopic composition of precipitation from two extratropical cyclones. *Mon. Weather Rev.*, 118:495–509.

Lovenduski, N. S. and Ito, T. (2009). The future evolution of the Southern Ocean CO2 sink. *J. Mar. Res.*, 67:597–617.

Madonna, E., Wernli, H., Joos, H., and Martius, O. (2014). Warm conveyor belts in the ERA-Interim dataset (1979-2010). Part I: Climatology and potential vorticity evolution. *J. Clim.*, 27:3–26.

Merlivat, L. and Jouzel, J. (1979). Global climatic interpretation of the Deuterium-Oxygen18 relationship for precipitation. *J. Geophys. Res.*, 84:5029–5033.

Papritz, L., Pfahl, S., Rudeva, I., Simmonds, I., Sodemann, H., and Wernli, H. (2014). The role of extratropical cyclones and fronts for Southern Ocean freshwater fluxes. *J. Clim.*, 27:6205–6224.

Papritz, L., Pfahl, S., Sodemann, H., and Wernli, H. (2015). A climatology of cold air outbreaks and their impact on air-sea heat fluxes in the high-latitude South Pacific. *J. Clim.*, 28:342–364.

Pfahl, S., Madonna, E., Boettcher, M., Joos, H., and Wernli, H. (2014). Warm conveyor belts in the ERA-Interim dataset (1979–2010). Part II: Moisture origin and relevance for precipitation. *J. Clim.*, 27:27–40.

Pfahl, S. and Wernli, H. (2008). Air parcel trajectory analysis of stable isotopes in water vapor in the eastern Mediterranean. *J. Geophys. Res. Atmos.*, 113:D20104.

Pfahl, S., Wernli, H., and Yoshimura, K. (2012). The isotopic composition of precipitation from a winter storm-a case study with the limited-area model COSMOiso. *Atmos. Chem. Phys.*, 12:1629–1648.

Raveh-Rubin, S. (2017). Dry intrusions: Lagrangian climatology and dynamical impact on the planetary boundary layer. *J. Clim.*, 30:6661–6682.

Rouault, M., Reason, C. J., Lutjeharms, J. R., and Beljaars, A. C. (2003). Underestimation of latent and sensible heat fluxes above the Agulhas Current in NCEP and ECMWF analyses. *J. Clim.*, 16:776–782.

Rouault, M., White, S. A., Reason, C. J. C., Lutjeharms, J. R. E., and Jobard, I. (2002). Ocean–Atmosphere interaction in the Agulhas Current region and a South African extreme weather event. *Weather Forecast.*, 17:655–669.

Sodemann, H., Schwierz, C., and Wernli, H. (2008). Interannual variability of Greenland winter precipitation sources: Lagrangian moisture diagnostic and North Atlantic Oscillation influence. *J. Geophys. Res. Atmos.*, 113:D03107.

Sprenger, M. and Wernli, H. (2015). The LAGRANTO Lagrangian analysis tool - Version 2.0. *Geosci. Model Dev.*, 8:2569–2586.

Talley, L. D. (2008). Freshwater transport estimates and the global overturning circulation: Shallow, deep and throughflow components. *Prog. Oceanogr.*, 78:257–303.

Uemura, R., Matsui, Y., Yoshimura, K., Motoyama, H., and Yoshida, N. (2008). Evidence of deuterium excess in water vapor as an indicator of ocean surface conditions. *J. Geophys. Res. Atmos.*, 113:D19114.

Wernli, H. and Davies, H. C. (1997). A Lagrangian-based analysis of extratropical cyclones. I: The method and some applications. *Q. J. R. Meteorolog. Soc.*, 123:467–489.

Wernli, H. and Schwierz, C. (2006). Surface cyclones in the ERA-40 dataset (1958–2001). Part I: Novel identification method and global climatology. *J. Atmos. Sci.*, 63:2486–2507.

[1]: ACE Expedition (2016), ACE Expedition - A better understanding of Antarctica, Swiss Polar Institute, Lausanne, Switzerland, accessed March 29, 2019,
<http://spi-ace-expedition.ch>

[2]: Isotope Hydrology Section IAEA (2015), Water Resources Programme - Global Network of Isotopes in Precipitation, International Atomic Energy Agency, Vienna, Austria, accessed March 29, 2019,
<http://www-naweb.iaea.org/napc/ih/IHS_resources_gnip.html>

[3]: South African Weather Service SAWS, Pretoria, South Africa, accessed March 29, 2019,
<http://www.weathersa.co.za/>

A

Influence of CAA and WAA on the Hydrological Budget

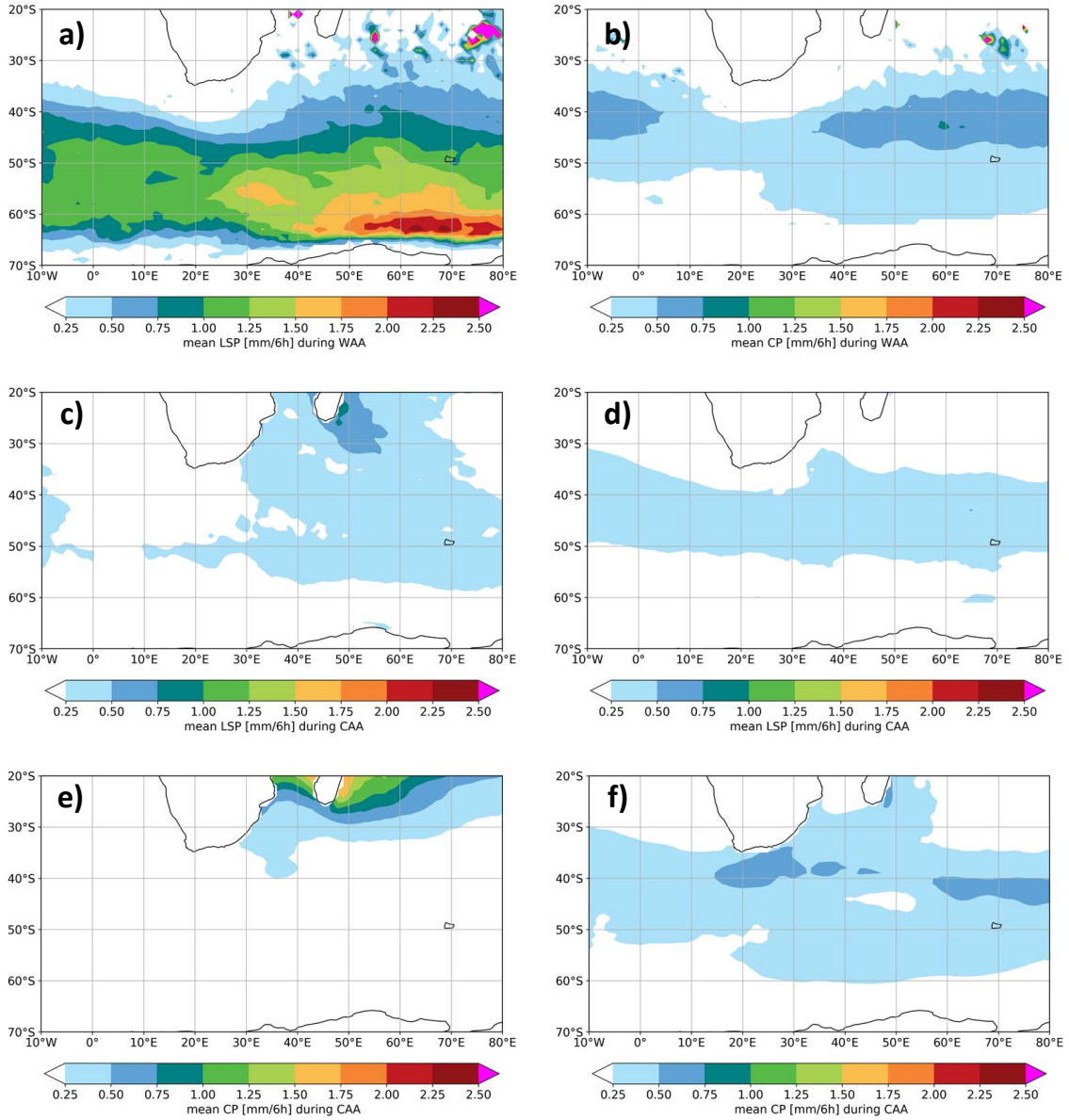

Figure A.1: Contour plots of the mean (a) LSP during WAA in DJF, (b) CP during WAA in JJA, (c) LSP during CAA in DJF, (d) LSP during CAA in JJA, (e) CP during CAA in DJF, (f) CP during CAA in JJA. The unit is mm/6h.

Figure A.1 shows additional seasonal mean values of CP and LSP during CAA and WAA, respectively.

Table A.1: Proportional share of the different advection types for CP, LSP, D and E as yearly average, from ECMWF reanalysis data between January 1979 and December 2016.

variables	**CAA**	**strong**	**weak**	**WAA**	**strong**	**weak**	**ZAA**
CP	54%	33%	21%	13%	7%	6%	33%
LSP	35%	21%	14%	26%	13%	13%	39%
D	0%	0%	0%	88%	64%	24%	12%
E	76%	52%	24%	1%	0%	1%	23%

Table A.1 shows the yearly averaged proportional share of CAA, WAA and ZAA for CP, LSP, E and D. The share for CAA and WAA is further subdivided into conditions of strong and weak CAA and WAA, respectively.

B

Moisture Source Conditions for Marion Island

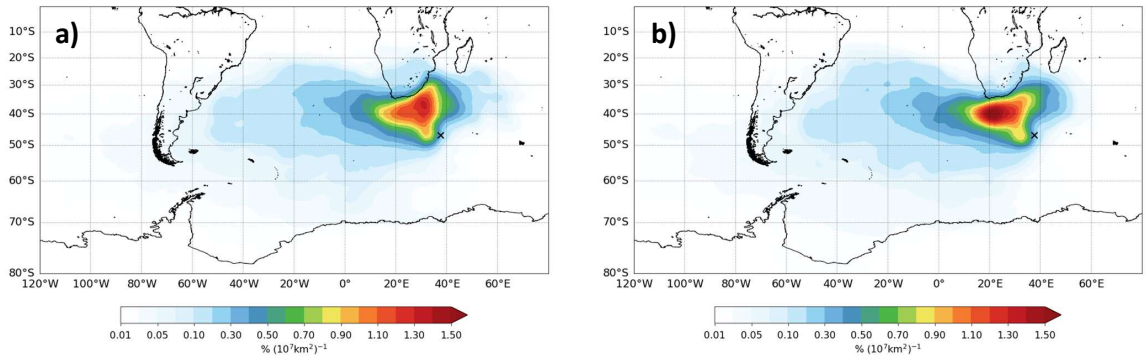

Figure B.1: Moisture uptake (% per 10^7km^2; shaded) for P on MI (black cross) for (a) MAM and (b) SON.

Figure B.1 shows seasonal means for the moisture source for precipitation on Marion Island for autumn and spring.

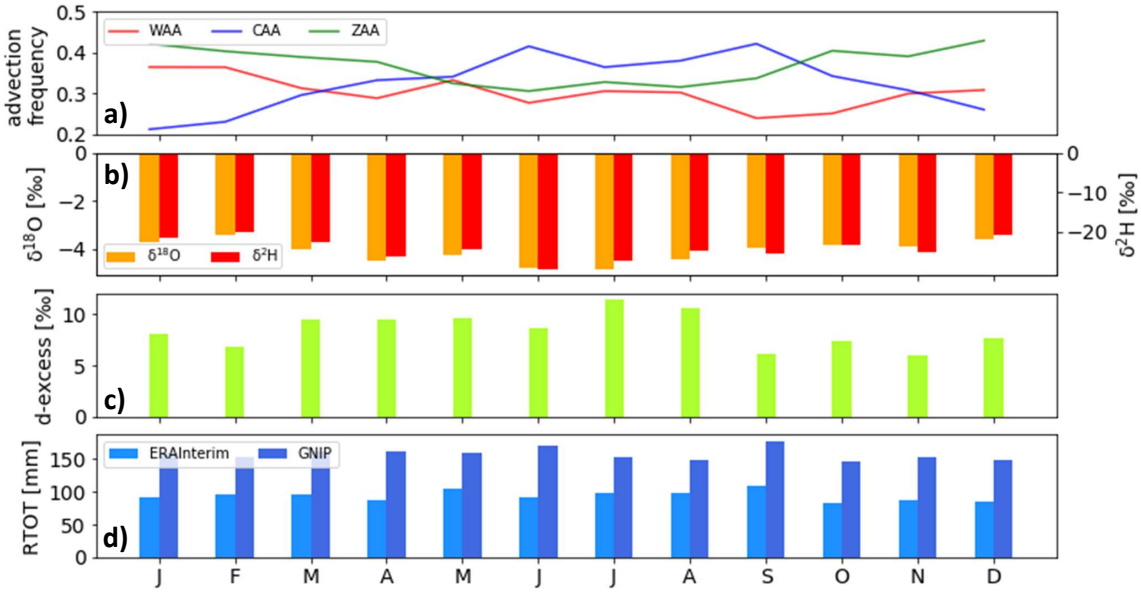

Figure B.2: Overview of GNIP and ERA-Interim data. (a) Line plot of monthly frequencies of WAA, CAA and ZAA. (b) Bar plot of monthly δ^{18}O (orange) and δ^2H (red) measurements on MI. (c) Bar plot of monthly d measurements on MI. (d) Box plot of monthly accumulated precipitation measured on MI (dark blue) and calculated in ERA-Interim (light blue).

Figure B.2 shows monthly WAA, CAA and ZAA frequencies on Marion Island as well as monthly SWI measurements measured on MI between 1993 and 2013 and monthly precipitation on MI, comparing the measured data from the GNIP data set with ERA-Interim reanalysis data. A permanent bias can be observed for the precipitation data, resulting from orographic enhanced P on MI due to its topography, which is not resolved in the ERA-Interim data set.

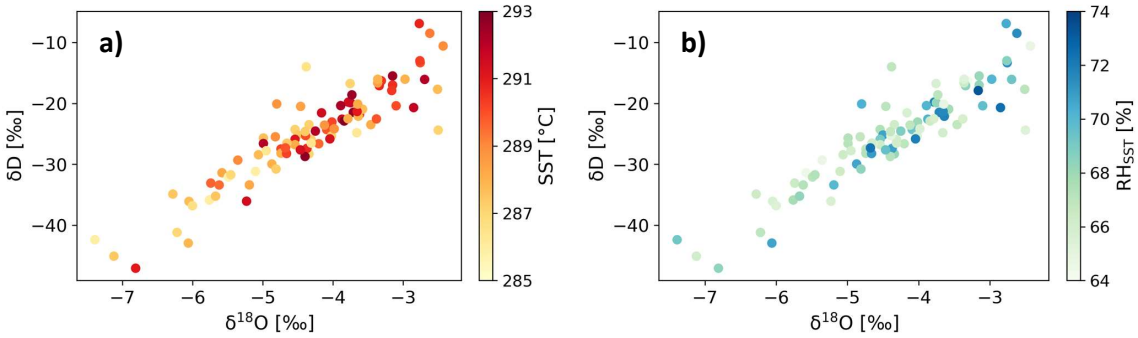

Figure B.3: Scatter plot of monthly measurements of δ^{18}O and δD on MI, colored according to the (a) SST (°C) and (b) RH_{SST} (%) at the moisture source.

Figure B.3 shows monthly SWI measurements on Marion Island linked to the conditions at the moisture source for MI in the form of SST and RH_{SST}.

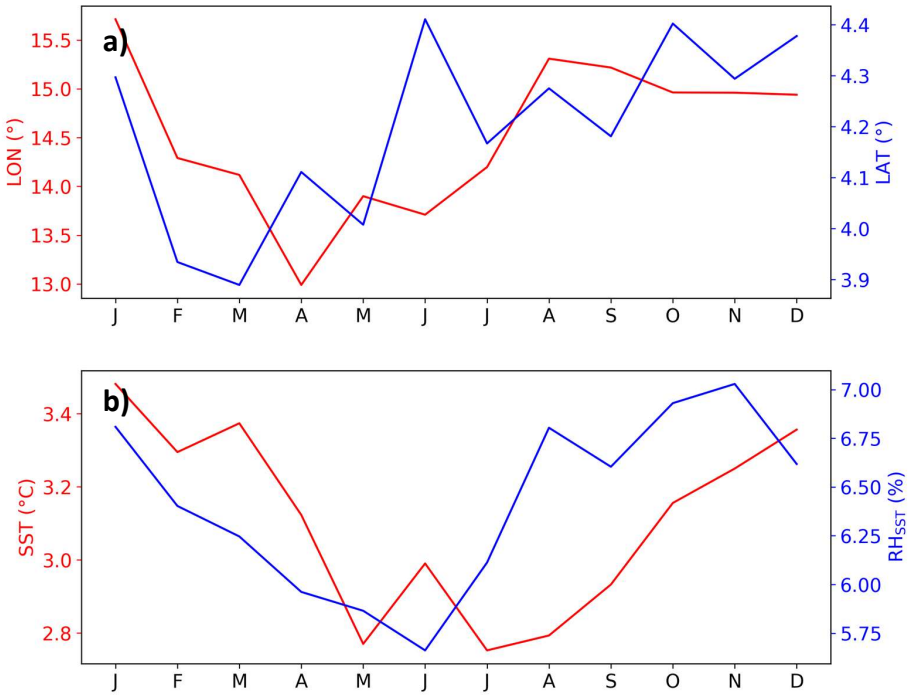

Figure B.4: Monthly standard deviation at the moisture source of MI for (a) longitude (°; red line) and latitude (°; blue line) and (b) SST (°C; red line) and RH_{SST} (%; blue line).

Figure B.4 shows the monthly standard deviation of longitude, latitude, SST and RH_{SST} at the moisture source for MI.